Vacuum membrane distillation for the production of ammonia fuel gas for solid oxide fuel cells

Influence of feed temperature and ammonia concentration on permeate quantity and quality

Evelien L.J. Martens

Delft University of Technology

TU Delft Delft University of Technology

Challenge the future

Vacuum membrane distillation for the production of ammonia fuel gas for solid oxide fuel cells

Influence of feed temperature and ammonia concentration on permeate quantity and quality

By:

Evelien Louise Josefien Martens

For the degree of:

Master of Science in Civil Engineering

Graduation committee:

Prof. Dr. Ir. Jules van Lier (Delft University of Technology, Department of Sanitary Engineering)
Dr. Ir. Henri Spanjers (Delft University of Technology, Department of Sanitary Engineering)
Ir. Niels van Linden (Delft University of Technology, Department of Sanitary Engineering)
Ir. Pieter Swinkels (Delft University of Technology, Department of Chemical Engineering)
Ir. Lex van Dijk (BLUE-tec Process Water Technologies)

Department of Sanitary Engineering, Department of Watermanagement

Faculty of Civil Engineering and Geosciences

Delft University of Technology, Delft

October, 2017

Abstract

Nitrogen (N) in the form of the reduced species ammonia (NH_3) is an energy carrier, an essential component of fertilizers and a basic building block in the chemical industry. It is the world's second most produced chemical and 1–2 % of the world's annual energy supply goes to the Haber-Bosch process, which converts atmospheric N into NH_3. N components ultimately end up in waste streams, for example after use of chemical products or protein degradation by organisms. They have to be removed at wastewater treatment plants (WWTPs), as discharging water with high N concentrations on surface waters may lead to eutrophication and thereby to a decrease in biodiversity.

Conventional technologies for N removal are mostly based on biological nitrification-denitrification processes and require energy and a carbon source. The newly developed Anammox process is common for sidestream N removal and achieves a substantial energy reduction, but does not recover nor utilize the removed N. The PhD project *From pollutant to power* aims for a paradigm shift in which N in residual streams is no longer regarded as a pollutant, but as an energy source instead. The novel concept underlying the PhD project is the idea that N in waste streams can be converted into electricity using a solid oxide fuel cell (SOFC). Costs and energy for nitrification-denitrification processes and Anammox can be saved and even better, energy can be produced. The overall goal is to develop a net energy producing system, in which NH_3 is extracted in gaseous form from high N and low carbon (C) waste streams through various chemical and/or physical concentration and separation steps and introduced into an SOFC for energy production. A NH_3 mass percentage of 10 is required in the fuel gas in order for an SOFC to function. WWTP reject water and urine are recognized as potential sources of N for energy recovery due to their relatively high N concentrations of 1.5 and 6 g total ammonia nitrogen (TAN)/L, respectively.

The master thesis research presented in this report focused on the technology of membrane distillation (MD) to determine its suitability for the gas production step within the *From pollutant to power* project. MD was selected for research because of its potentially low energy requirement, because the applied membranes have proved to be stable and because of promising concentration factors presented in literature. However, due to knowledge gaps in literature, it could not be predicted whether or not a 10 mass percentage NH_3 fuel would be obtainable with MD for reject water and urine.

In MD, the driving force for gas transport through hydrophobic, microporous membranes is a vapor pressure difference over the membrane pore entrances. The research objective of this study was to determine the influence of feed temperature and ammonia concentration on permeate quantity and quality in vacuum membrane distillation for the production of an ammonia fuel gas for solid oxide fuel cells, and to determine the suitability of MD as technology for gas extraction within the *From pollutant to power* project. Synthetic ammonium bicarbonate (NH_4HCO_3) solutions were used to simulate (concentrated) reject water and urine in simulations and laboratory experiments. Simulations were carried out with the code PHREEQC in order to estimate vapor pressures in feed solutions and to determine which test conditions would be favorable for NH_3 transport over the transport of other volatile components in the feed solution (H_2O and CO_2).

Selected test conditions were pH 10 to exclude CO_2 gas transfer and temperatures from 25–55 °C to maximize the NH_3 fraction in the permeate gas. Feed solutions with TAN concentrations of 1.5, 12 and 20 g/L were selected for the experiments, from which total and NH_3 transmembrane fluxes were determined. Results of the laboratory experiments showed that it is possible to obtain a fuel gas

quality of 10 mass percentage NH_3 for low temperatures (25 – 35 °C) and a high TAN concentration (20 g/L). At higher temperatures and lower concentrations, permeate NH_3 mass percentages were lower than 10. A global mass transfer coefficient including resistances in feed, membrane and permeate was determined. Higher resistance to mass transfer was observed at higher temperatures due to increased polarization effects, resulting in lower transmembrane fluxes. The effect of polarizations was stronger for NH_3 than for H2O. The need of a preceding concentration step in case MD is applied for SOFC fuel production is proved, as 1.5 and 12 g TAN/L solutions did not result in a permeate gas quality sufficient for the gas to be fed directly to an SOFC.

In conclusion, it was possible to create an SOFC NH_3 fuel of sufficient quality on conditions of a preceding concentration step, basic conditions and low applied temperatures. To determine whether or not MD is a suitable technique within the *From pollutant to power* project, an overall mass and energy balance including results from concentration step and SOFC research must be considered. As low temperature ranges are favorable both in terms of energy requirement and permeate gas quality and energy is considered an important parameter within the project, MD might be a suitable option for gas production.

Acknowledgement

Finishing my master studies in Sanitary Engineering at Delft University of Technology within the *From pollutant to power* project has resulted in a period full of discoveries and possibilities. Although it was hard (work) at times, I have enjoyed it.

Firstly, I would like to thank Ir. Niels van Linden, my daily supervisor, who was always available for questions, answers and discussions. I have learned a lot from him in the past months.

Also, I would like to thank the other members of my graduation committee, Prof. Dr. Ir. Jules van Lier, Dr. Ir. Henri Spanjers, Ir. Pieter Swinkels and Ir. Lex van Dijk, for their critical comments and useful suggestions during the kick-off, midterm and greenlight presentations. It is always good to get a fresh view on things! Thanks to Mohammed Jafar and Armand Middeldorp, staff in the Sanitary Engineering water laboratory, for their support and for making the experiments a little bit easier.

Finally, I would like to thank my family and my roommates for all the tea and food that magically appeared on my desk when I was studying at home. And of course my study mates and those special friends, that can always make a long day in the lab or behind the computer a little lighter.

Contents

Chapter 1

Introduction

1.1 Background: *From pollutant to power*

1.1.1 Ammonia contamination and removal

Nitrogen (N) in the form of the reduced species ammonia (NH_3) is an energy carrier, an essential component of fertilizers and a basic building block in the chemical industry. It is the world's second most produced chemical and one to two percent of the world's annual energy supply goes to the Haber-Bosch process [61,1], which converts atmospheric N into NH_3 by a reaction with hydrogen (H_2) under high temperatures (400–500 °C) and pressures (15-25 MPa) [66]. N components ultimately end up in waste streams, for example after use of chemical products or protein degradation by organisms (Figure 1.1). These components have to be removed at wastewater treatment plants (WWTPs), as discharging water with high N concentrations on surface waters may lead to eutrophication and thereby to a decrease in biodiversity. In the Netherlands, standard effluent requirements regarding N demand removal to achieve a total N concentration lower than 10 mg/L and regarding ammonium (NH_4^+) a concentration lower than 1 mg NH_4^+–N/L is required [1].

Conventional technologies for waterline N removal are mostly based on biological nitrification-denitrification processes. The energy demand for aeration to facilitate nitrification can mount to 70% of the total energy usage of a WWTP [3] and a carbon source is required for denitrification. In the Netherlands, yearly costs of N removal from municipal wastewater by nitrification-denitrification processes are 267 to 445 million euros [67]. In addition, the byproduct greenhouse gas N_2O is released into the atmosphere during denitrification [7]. The newly developed Anammox (anaerobic ammonia oxidation) process is common for sidestream N removal and achieves a substantial energy reduction of up to 60% in comparison to conventional technologies [9,10,63]. Moreover, Anammox does not require an external carbon source and results in a lower sludge production [10,63]. However, also the Anammox process does not recover nor utilize the removed N. Moreover, in practice it is difficult to start up and a stable long-term operation is not always guaranteed due to the use of slow-growing, sensitive organisms. The Anammox process for treating the main sewage stream at ambient temperature does not exist yet [64,65]. When conventional processes or Anammox are applied, energy is consumed for both NH_3 production and removal.

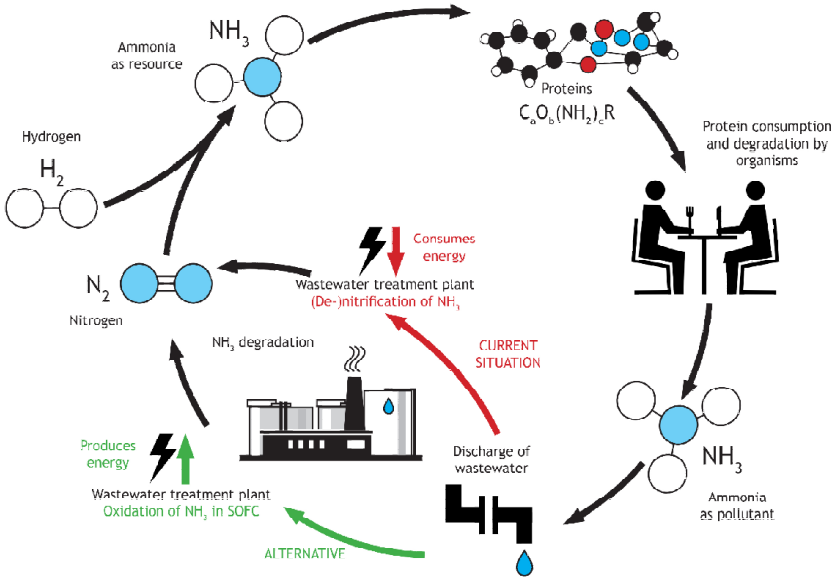

Figure 1.1: Ammonia cycle with current and alternative treatment routes [2]

Both conventional technologies and Anammox degrade N compounds into N_2 gas that is disposed of by releasing it into the atmosphere, ignoring the stored chemical energy in ammonia. According to the European Unions Waste Framework Directive, disposal is the least preferred option of handling waste (Figure 1.2) [4]. Considering that residual streams containing N are present and that direct re-use is not possible, recycling of NH_3 would be the preferred option. Onsite recovery of NH_3 in a recyclable form is challenging because of possible contaminations, because it requires a market outlet that has not been established and because it often involves an extra energy demand in the form of wheel transport [10]. Therefore, recycling is not always feasible or desirable.

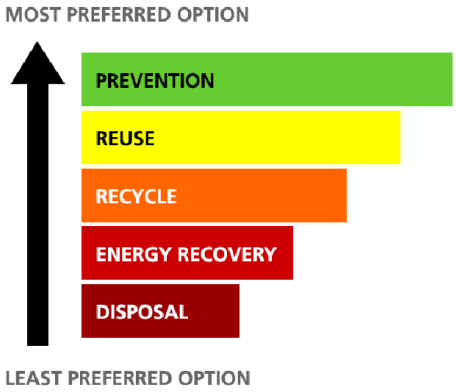

Figure 1.2: Waste hierarchy

1.1.2 Ammonia as fuel for solid oxide fuel cells

The PhD project *From pollutant to power* aims for a paradigm shift in which N in residual streams is no longer regarded as a pollutant, but as an energy source instead. Innovations so far have merely focused on reducing the energy consumption for conventional N removal technologies; no existing project recognizes reduced N as a potential energy source [1]. The novel concept underlying the *From pollutant to power* project is the idea that N in waste streams can be converted into electricity using a solid oxide fuel cell (SOFC), acknowledging the energy stored in NH_3. Costs and energy for nitrification-denitrification processes and Anammox can be saved and even better, energy can be produced with a potential value of 32 million euros per year [1]. Moreover, as recycling is not always feasible or desirable, onsite NH_3 valorization in the form of energy recovery might form an attractive alternative even though it is considered less favorable in the European Unions Waste Framework Directive. Additional advantages are that more carbon source is available for biogas production in absence of denitrification, thereby increasing the energy potential of the treated waste stream [1], and that leakage of the denitrification byproduct greenhouse gas N_2O into the atmosphere is reduced.

Fuel cells are devices that convert the chemical energy of gaseous or liquid compounds into electrical energy by a chemical reaction with an oxidizing agent [6]. An SOFC works at temperatures above 500 °C, at which NH_3 gas is cracked into H_2 in the presence of a catalyst (Appendix A1). The decomposition of ammonia is both sufficient and fast at SOFC operating temperatures. Therefore, NH_3 can be fed as fuel to an SOFC directly and cell performance is similar to that obtained under pure H_2 [69,70]. Nowadays, the use of conventional energy technologies is under pressure and a shift is made in the direction of renewable energy sources. NH_3 can take a role as renewable energy carrier and the interest in its usage as source of H_2 in fuel cells increases [1,68,73]. Pure NH_3 is easy to produce, store and transport. It can be liquefied at ambient temperature under a pressure of 10 atm or under ambient pressure at a temperature of about −33 °C [68] and the volumetric energy density of liquefied NH_3 is higher than that of liquid H_2. It can be dissolved in water up to very high levels (circa 30% by volume), offering further advantages for transport [73,74]. Moreover,

its usage is relatively safe because NH_3 is less flammable than other fuels and because any leakage can be detected easily due to its pungent odor [68]. Since byproducts of cell reactions are merely N and H_2O, no greenhouse gases are emitted [74].

The performance and durability of SOFCs are affected by the presence of impurity species in fuels [69]. The impact of major impurities such as sulphur (S) and carbon (C) has been studied by researchers. S compounds lead to poisoning of SOFC catalysts, which is in most cases irreversible. C depositions result in coking and SOFC deactivation. Impact of trace impurities such as phosphorus is still unclear. In general, water vapor, inert gases and biogas are allowed in SOFCs, whereas introduction of oxidizing agents, salts and solids should be avoided and impurities should be removed or minimized [69]. Available information on SOFC performance for fuel mixtures with NH_3 concentrations lower than 25% is limited.

1.1.3 *From pollutant to power* research tracks

Summarizing, *From pollutant to power* might offer an attractive alternative to conventional and Anammox processes for N removal, recovering energy from NH_3 (Figure 1.1). *From pollutant to power* is divided into two research tracks that differ in the type of waste streams they address. The first track concerns waste streams with both a high N and a high C concentration and is executed at Katholieke Universiteit Leuven, Department of Chemical Engineering, Process and Environmental Technology Lab. The second track concerns waste streams with high N and low C concentration and is executed at Delft University of Technology, Department of Water Management, section Sanitary Engineering [1]. The master thesis research presented in this report is part of the latter.

Streams with high N concentrations are addressed because it is considered more feasible to recover N from these streams instead of directly from the municipal wastewater. Nonetheless, it is expected that project results will contribute to the development of technologies focusing on direct N extraction from sewage [1]. Residual streams with high N and low C concentrations that the second track of the PhD project focuses on, are WWTP reject water and urine. WWTP reject water is the internal liquid flow resulting from dewatering of anaerobically digested sludge. It has a total ammonia nitrogen (TAN; defined as the sum of NH_3 and NH_4^+) concentration of up to 1.5 g/L, originating from organic N present in biomass that is released and transformed to NH_3 and NH_4^+ during anaerobic digestion [9,10]. Reject water is either returned to the start of a WWTP to remove TAN, increasing the wastewater influent N load up to 25% [1], or treated in sidestream processes [9,10]. Urine, with a TAN concentration of up to 6 g/L after hydrolysis, contributes to only 1% of the total wastewater flow in volume and is currently only exceptionally collected separately in the Netherlands. However, as 80% of the total N content in municipal wastewater originates from urine, it is identified as a potential stream for N recovery [71]. Since industrial effluents contribute to wastewater contaminations by NH_3 or N compounds [11], it is expected that industrial wastewater effluent streams with high N concentration will be identified during the project as well.

The second track of the PhD project *From pollutant to power* is on its turn divided into five research tracks (Figure 1.3). Through various chemical and/or physical concentration and separation steps, gaseous NH_3 is extracted from the high N and low C waste streams and fed to an SOFC for energy production. SOFC electrical and thermal energy can be used for the concentration and gas extraction steps. The overall goal is to develop a net energy producing system, in which the energy that is required to produce the fuel is less than the energy produced from the fuel.

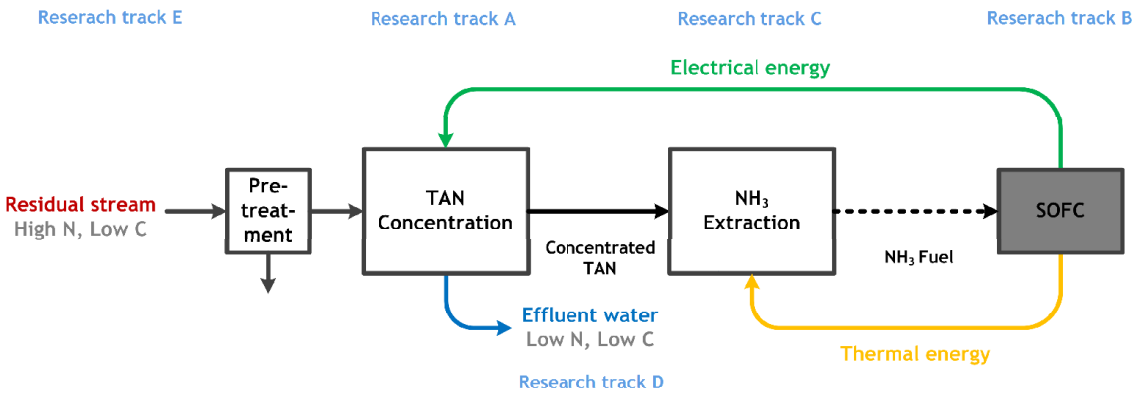

Figure 1.3: Research tracks A: Selection of most suitable technology for TAN concentration; B: Evaluation of SOFC performance on the produced NH_3 fuel; C: Selection of most suitable technology to produce gaseous NH_3; D: Development of a mass and energy balance tool and E: System implementation and determination of required pre-treatment for various residual water streams. Adapted from [2].

1.2 Membrane distillation

The master thesis research presented in this report is part of research track C in Figure 1.3, which is the NH_3 extraction or gas production step. It focuses on the technology of membrane distillation (MD), to determine its suitability for the production of an SOFC fuel gas from residual streams with high N and low C concentration (reject water and urine). MD was selected for further research based on its advantages compared to conventional gas removal technologies (explained in paragraph 1.2.1) and on concentration factors found in literature (explained in paragraph 1.2.2).

1.2.1 Process and advantages

MD is a separation technology in which a watery solution flows past a hydrophobic, microporous membrane. Due to the hydrophobic nature of the membrane created by surface tensions in the membrane material, gas molecules of volatile components can be transported through the membrane while liquids cannot enter the dry, gas-filled pores [12]. The membrane pore size, in the order of magnitude of micrometers, is large in comparison to the kinetic diameter of gas molecules (0.265 nm and 0.326 nm for H_2O and NH_3, respectively [13]). Therefore, there is no interaction between the membrane material and the transported gas molecules (Figure 1.4); the membrane merely acts as a support for the vapor-liquid interface [13,14]. The driving force in MD is a transmembrane vapor pressure difference, induced by temperature and concentration differences at membrane pore entrances. The four most commonly applied configurations to maintain this vapor pressure difference, varying in the way that permeated gas is transported out of the membrane module, are direct contact membrane distillation (DCMD; the permeated component condenses directly in a liquid coolant flowing through the module at permeate side), air gap membrane distillation (AGMD; the permeated component passes through a layer of static gas, condenses within the membrane module and is drained out of the module by gravity), sweeping gas membrane distillation (SGMD; the permeated component is swept out of the module by a carrier gas stream) and vacuum membrane distillation (VMD; a vacuum pressure is maintained on the permeate side) [12] (Figure 1.5).

MD has received attention for the removal of volatile compounds like NH_3 because of its potentially low energy requirement. It has advantages of mild operation conditions of atmospheric pressure and temperatures lower than the boiling points of the components to be removed, the possibility to utilize low-grade heat or alternative energy sources (such as solar and geothermal energy), controlled separation of liquid feed and gas permeate streams and a small installation footprint (high surface-to-volume ratio) [12,15,16]. Compared to conventional gas removal technologies such as

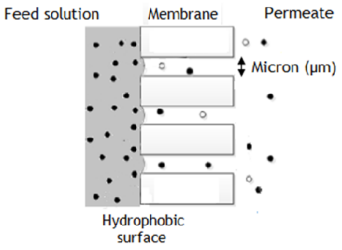

Figure 1.4: Hydrophobic, microporous MD membrane [13]; filled rounds represent NH_3 molecules and open rounds H_2O molecules.

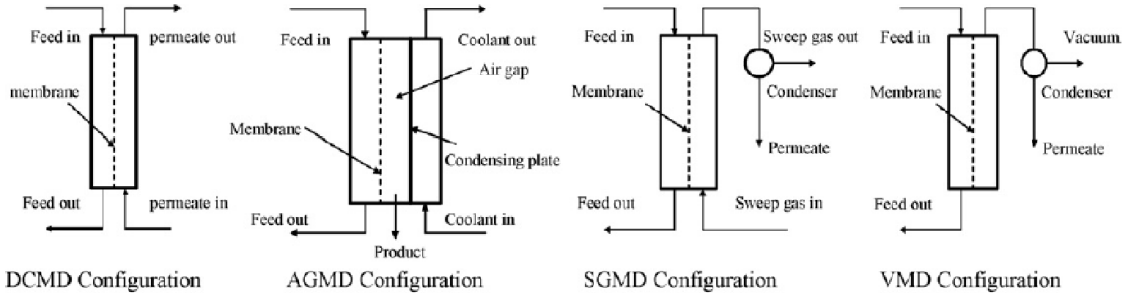

Figure 1.5: MD configurations [12]

direct distillation and gas or steam stripping, MD has fulfilled the requirements of process intensification. This means that equipment size shrinks substantially, energy consumption is reduced, plant efficiency is boosted and/or waste production is minimized and results in a smaller, cleaner, more energy efficient and more productive technology [13]. MD has mainly been examined and found to be applicable for the production of high purity water, desalination and concentration processes in various industries [12]. Membranes are widely available and have proved to be stable. Hydrophobicity was maintained and membrane properties were unchanged in the MD temperature range of 20-80 °C and in experiments that lasted longer than a year [12,19].

1.2.2 Knowledge gap

Literature research underlines the relevance of investigation of MD for NH_3 SOFC fuel gas production. Research on MD in relation to NH_3 recovery has mainly been focused on DCMD, in which NH_3 gas is absorbed in an acid solution on the permeate side of the membrane. Typically sulfuric acid (H_2SO_4) is used, which leads to formation of ammonium sulfate ($(NH_4)_2SO_4$) that can be used for fertilizer production [20]. Only SGMD and VMD configurations result in a gaseous permeate, as is required in the *From pollutant to power* project. Research on MD in relation to N recovery in the form of NH_3 gas has been focused on gas removal instead of on gas production. In gas removal the feed solution is the intended product, whereas in gas production the intended product is the permeate gas. There is a lack of information on permeate composition in general and as mainly higher temperature ranges (above 45 °C) have been tested, there is also a lack of information on gas transport in lower temperature ranges (below 45 °C). Moreover, applied test conditions are often unclear, research has been carried out unsystematically (multiple parameters varied at the same time), system settings are not well-reasoned, focus has been put on determination of membrane characterization factors that do not directly offer numbers usable in practical design, test solutions have much lower (100 mg/L) or higher (180 g/L) concentrations than expected in (concentrated) reject water and urine and/or no direct relation is given between driving force (vapor pressure difference) and permeate quantity and quality [10-13,21-30]. Altogether, this makes it hard to interpret data available in literature and to use it in the *From pollutant to power*

project. Nonetheless, literature shows that MD could be a promising technology in the application of SOFC fuel gas production, with NH_3 concentration factors of up to 11 reported in literature for SGMD and VMD [17]. This will be explained further in paragraph 3.1.

1.3 Research plan

1.3.1 Research objective

A VMD configuration was selected for the master thesis research (explained further in paragraph 4.4). As it is known from literature that temperature and concentration differences at pore entrances are the drivers for gas transport in MD, temperature and TAN concentration were chosen as variables in experimental research. The research objective of the thesis presented in this report is formulated as:

"Determining the influence of feed temperature and ammonia nitrogen concentration on permeate quantity and quality in vacuum membrane distillation for the production of an ammonia fuel gas for solid oxide fuel cells from an ammonium bicarbonate solution simulating (concentrated) reject water and urine."

Permeate quantity is defined as the absolute total flux (total mass transport per unit of membrane surface area and time; J_{tot}) that is transferred through the membrane. Permeate quality is defined as the mass percentage of NH_3 (m% NH_3) in the permeate gas:

$$\text{m\% NH}_3 = \frac{\text{mass}_{\text{NH}_3,\text{permeate}}}{\text{mass}_{\text{total,permeate}}} \cdot 100\% \tag{1.1}$$

1.3.2 Research questions and approach

The objective is addressed through answering the following research questions and sub-questions:

1. How do temperature and ammonia nitrogen concentration influence permeate quantity and quality in vacuum membrane distillation (at selected test conditions)?
2. Could membrane distillation be a suitable technology for the production of an ammonia fuel gas for solid oxide fuel cells within the *From pollutant to power* project?
   (a) What is the permeate quantity that can be obtained (at selected test conditions)?
   (b) What is the permeate quality that can be obtained (at selected test conditions)?
   (c) What are considerations regarding energy?

Answers to these questions are obtained through literature research, PHREEQC simulations and laboratory scale experiments.

1.3.3 Assumptions and boundary conditions

Several assumptions and boundary conditions related to the incoming feed water and outgoing permeate gas of the MD gas production step are:

- *Influent concentration:*
  It is assumed that a concentration step can be included before the gas production step (Figure 1.3). This means that TAN concentrations in the MD gas production step feed solution can be higher than concentrations in reject water (1.5 g/L) and urine (6 g/L);
- *SOFC fuel requirements:*
  A gaseous SOFC fuel with a minimum of 5–10 m% NH_3 is required (Appendix A2). Water vapor, inert gases and biogas are allowed in the SOFC fuel gas;

- *Available energy:*
  Energy available for the MD gas production step is SOFC thermal energy, contained in SOFC outlet gases.

Chapter 2

Theoretical background

2.1 Membrane distillation feed solution

2.1.1 Reject water and urine characteristics

Reject water originating from dewatering of anaerobically digested sludge contains a significant amount of N, as organic N is degraded and released into the liquid phase as NH_4^+ and NH_3 during the anaerobic digestion process. TAN concentrations typically go up to 1.5 g/L [10]. Due to the retention of carbon dioxide (CO_2) in the digester bulk liquid to balance the positively charged NH_4^+ ion at the typical pH range prevailing in digesters (7.2-7.8), alkalinity concentration is high. Reject water alkalinity primarily exists in the form of bicarbonate (HCO_3^-). Other characteristics of reject water streams include the presence of suspended solids, some biochemical oxygen demand and orthophosphates [10,34].

As noted in paragraph 1.1, 80% of the total N load in municipal wastewater originates from urine. Although the composition will vary for each individual, approximated properties and an overall composition of urine are presented in literature. Urine consist for about 95% of water and 5% of solids, with urea (CON_2H_4) and sodium chloride (NaCl) as main compounds [10]. Moreover, it contains potassium (K), calcium (Ca), sulphate (SO_4^{2-}) and phosphates ($H_2PO_4^-$, HPO_4^{2-} and PO_4^{3-}) [10, 31-33]. The CON_2H_4 concentration in urine typically is 20 g/L [10]. CON_2H_4 is hydrolyzed and decomposed naturally within several days, resulting in a concentration of 5-6 g TAN/L [32]. During hydrolysis also HCO_3^-)is released, resulting in a buffer solution [10,31-33].

2.1.2 Feed solution equilibria and influence of ionic strength

When MD is applied as extraction technology to produce NH_3 gas from reject water or urine, a concentration step is required (further explained in paragraph 3.1). A concentration step will change the original reject water or urine composition. Because the technology to be used for concentration purposes has not been defined yet, the exact water matrix of the MD feed solution is still uncertain. In this master thesis study, ammonium bicarbonate (NH_4HCO_3) solutions were used to simulate reject water and urine, as NH_4HCO_3 is the main form in which TAN appears in these streams (paragraph 2.1.1).

When NH_4HCO_3 is brought into solution in the concentration range found in reject water and urine, it will dissociate in NH_4^+ and HCO_3^- ions [23]:

$$NH_4HCO_3(s) \xrightarrow{H_2O} NH_4^+(aq) + HCO_3^-(aq) \tag{2.1}$$

This results in three equilibria of main importance in the feed solution, namely the ionization equilibrium of water, the TAN equilibrium and the total inorganic carbon (TIC) equilibrium. Before discussing these equilibria, it is explained how the ionic strength of a solution influences the distribution of species in a solution under equilibrium conditions.

Influence of ionic strength on equilibrium species distribution

Any chemical equilibrium can be described by the law of mass action. A chemical equilibrium reaction can be written in generalized form:

$$aA + bB \leftrightarrow cC + dD \tag{2.2}$$

According to the law of mass action, the distribution of the species in the reaction can be described by a thermodynamic equilibrium or dissociation constant:

$$K = \frac{[C]^c[D]^d}{[A]^a[B]^b} \tag{2.3}$$

In this formula, [A], [B], [C] and [D] are activities of the chemicals A, B, C and D, respectively, and a, b, c, and d are stoichiometric coefficients [75].

Activity is a measure of the effective concentration of a species in a mixture. It corrects for

the non-ideality of solutions, taking interactions between molecules into account. In non-ideal solutions, electrostatic shielding occurs. Ions in solution are surrounded by water molecules and other dissolved ions that act as a shield and reduce the reactivity of the ion; the net charge of the atmosphere around the ions is less than the net charge of the ions, which attenuates attractions between positive and negative ions (relative to their attraction in pure distilled water). This electrostatic shielding effect can be corrected for by using an activity coefficient, that relates the activity of an ion to its molal concentration:

$$[i] = \gamma_i \cdot \mathrm{m}_i / \mathrm{m}_i^0 \equiv \gamma_i \cdot \mathrm{m}_i \tag{2.4}$$

In this formula, $[i]$ is the activity of ion i, γ_i its activity coefficient and m_i its molal concentration. The activity coefficient becomes dimensionless by division of the molal concentration with the standard state molal concentration (m_i^0 for ion i, i.e. 1 mol/kg H_2O). The activity coefficient depends on the ionic strength (I) of the solution, which can be calculated as:

$$I = \frac{1}{2} \sum (\mathrm{m}_i / \mathrm{m}_i^0 \cdot \mathrm{z}_i^2) \equiv \frac{1}{2} \sum (\mathrm{m}_i \cdot \mathrm{z}_i^2) \tag{2.5}$$

In this formula, z_i is the electric charge of ion i. Also I becomes dimensionless by division of the molal concentration with the standard state molal concentration. Equation 2.5 includes both concentration and charge and must take all major ions and charged complexes into account. The I of freshwater is normally less than 0.002, while seawater has an I of about 0.7 [75].

Various equations have been proposed for the calculation of activity coefficients. For dilute solutions with $I < 0.1$, the Debye-Hückel equation can be used [75]:

$$\log \gamma_i = -\frac{\mathrm{A} \mathrm{z}_i^2 \sqrt{I}}{1 + \mathrm{B} \mathring{\mathrm{a}}_i \sqrt{I}} \tag{2.6}$$

A and B are temperature dependent constants and å is an empirical ion-size parameter that is a measure of the effective diameter of the hydrated ion.

For I values between 0.1 and 1, a modified version of the Debye-Hückel equation can be used [75]:

$$\log \gamma_i = -\frac{\mathrm{A} \mathrm{z}_i^2 \sqrt{I}}{1 + \mathrm{B} \mathrm{a}_i \sqrt{I}} + \mathrm{b}_i I \tag{2.7}$$

A and B are the temperature dependent coefficients from the Debye-Hückel equation and a_i and b_i are ion-specific fit parameters [75]. Geochemical models also use more complicated Pitzer equations [83].

The net effect is that activity coefficients decrease with ionic strength up to $I \sim 0.7$. In solutions with higher values of I, activity coefficients may increase again. More water molecules act as a hydration shell around charged components and less free water is available as solvent. This effect is known as salting out and is also seen in the solution of gases.

In an ideal solution, all activity coefficients would be 1 (unity). Generally, deviations from ideal behavior tend to become larger (and activity coefficients tend to become smaller) with increasing molality and temperature [76]. For uncharged species and ions present at trace concentrations with no other ions in its surroundings, activity coefficients approximate unity. In that case, activity approximates molal concentration [75]. For pure solids, activities are unity [75] and the activity of H_2O in saline water can be calculated as well [77].

As activity coefficients must be known in order to calculate molal concentrations from an equilibrium constant, and activity coefficients depend on ionic strength that on its turn depends on concentrations, calculation of activities requires iteration [75]. Activity coefficients may also be determined experimentally; this is not further elaborated upon in this thesis. In the practice of

water treatment, often molar concentrations are used instead of activities in equilibrium calculations.

Ion activity is also influenced by the formation of aqueous complexes. The total elemental concentration of a component is higher than the free ion concentration when part of the component mass is present in aqueous complexes with other ions [75].

Water ionization equilibrium

In the water ionization equilibrium, liquid H_2O dissociates into equal amounts of hydrogen ions (H^+) and hydroxide (OH^-) ions:

$$H_2O(l) \leftrightarrow H^+(aq) + OH^-(aq) \tag{2.8}$$

The degree of dissociation is dependent on temperature and can be described by a thermodynamic equilibrium constant:

$$K_{eq,H_2O} = \frac{[H^+][OH^-]}{[H_2O]} \tag{2.9}$$

In this equation, $[H^+]$, $[OH^-]$ and $[H_2O]$ represent the activities of $H^+(aq)$, $OH^-(aq)$ and $H_2O(l)$, respectively. The water ionization equilibrium constant K_{eq,H_2O} decreases with increasing temperature [35].

Total ammonia nitrogen equilibrium

Ammonia nitrogen exists in aqueous solutions as NH_4^+ and NH_3 in equilibrium:

$$NH_4^+(aq) \leftrightarrow NH_3(aq) + H^+(aq) \tag{2.10}$$

The TAN equilibrium is mainly a function of temperature and pH and can be described by the following thermodynamic constant:

$$K_{eq,NH_4^+} = \frac{[NH_3][H^+]}{[NH_4^+]} \tag{2.11}$$

In this equation, $[NH_3]$, $[H^+]$ and $[NH_4^+]$ represent the activities of $NH_3(aq)$, $H^+(aq)$ and $NH_4^+(aq)$, respectively.

In alkaline solutions, NH_4^+ reacts with OH^- to form NH_3 and H_2O and the TAN equilibrium can be written as:

$$NH_4^+(aq) + OH^-(aq) \leftrightarrow NH_3(aq) + H_2O(l) \tag{2.12}$$

Both temperature and pH shift the equilibrium to the right side, favoring the formation of NH_3 [10,11,37]. In Figure 2.1, the TAN equilibrium is presented as the molar ratio of NH_3 over TAN. The equilibrium ratio is shown for TAN concentrations expected in reject water (1.5 g/L) and urine (6 g/L) as a function of pH for a low, medium and high temperature of the MD temperature range (20, 45 and 70 °C, respectively). It can be seen that the NH_3/TAN ratio is higher than 0.5 for pH values above 9.5 and that it approaches 1 for pH values higher than 11 for all three temperatures. The influence of solution ionic strength can be noticed as well. At higher TAN concentrations, I is higher and the reactivity of the ions NH_4^+ and OH^- is decreaesd. Thus, less NH_3 is formed. Figure 2.1 is the result of simulations in the code PHREEQC. In these simulations, HCl has been added to decrease pH and NaOH to increase pH when necessary to obtain the desired pH value.

Total inorganic carbon equilibrium

The TIC equilibrium is more complex, on itself consisting of multiple equilibria between H_2O and the species CO_2, carbonic acid (H_2CO_3), HCO_3^- and carbonate (CO_3^{2-}):

$$CO_2(aq) + H_2O(l) \leftrightarrow H_2CO_3(aq) \leftrightarrow H^+(aq) + HCO_3^-(aq) \leftrightarrow 2\,H^+(aq) + CO_3^{2-}(aq) \tag{2.13}$$

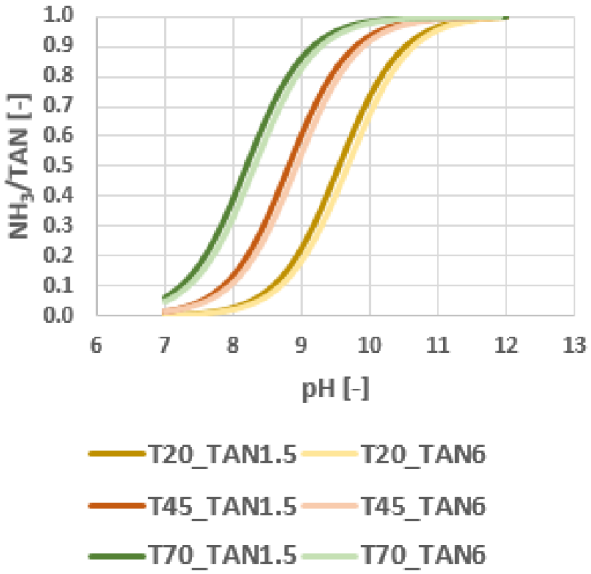

Figure 2.1: NH_3/TAN ratio obtained from PHREEQC simulations of NH_4HCO_3 solutions with NaOH and HCL additions for pH corrections.

The TIC equilibrium is mainly a function of pH and temperature. Its change over pH for temperature 25 °C is shown in Figure 2.2. At every pH, the H_2CO_3 concentration is assumed to be negligible compared to the concentration of CO_2 [78]. Therefore, TIC equilibrium concentrations (mol/L) can be described by:

$$C_{CO_2} = \frac{[H^+]^2}{[H^+]^2 + K_1[H^+] + K_1K_2} \cdot [TIC] \tag{2.14}$$

$$C_{HCO_3^-} = \frac{K_1[H^+]}{[H^+]^2 + K_1[H^+] + K_1K_2} \cdot [TIC] \tag{2.15}$$

$$C_{CO_3^{2-}} = \frac{K_1K_2}{[H^+]^2 + K_1[H^+] + K_1K_2} \cdot [TIC] \tag{2.16}$$

In these equations, K_1 is the equilibrium constant for the reaction expressed in Equation 2.17, K_2 the equilibrium constant for the reaction expressed in Equation 2.18 and [TIC] the total concentration of dissolved inorganic carbon in the system (mol/L) (i.e. the sum of the concentrations CO_2, HCO_3^- and CO_3^{2-}) [78].

$$CO_2(aq) + H_2O(l) \leftrightarrow H^+(aq) + HCO_3^-(aq) \tag{2.17}$$

$$HCO_3^-(aq) \leftrightarrow H^+(aq) + CO_3^{2-}(aq) \tag{2.18}$$

Also for the TIC equilibrium, activities of the species should be used instead of concentrations to calculate effective equilibrium concentrations when the solution cannot be considered an ideal solution.

Two things are of main importance regarding the TIC equilibrium. Firstly, because CO_2 is volatile, it can be transported through an MD membrane when it is present in a feed solution. This would influence the quality of the permeated fuel gas. As can be seen in Figure 2.2, only a small fraction of TIC is present as CO_2 for pH values above 8 [10,23,36].

Secondly, the presence of two pairs of a weak acid and a conjugated base make the feed solution a

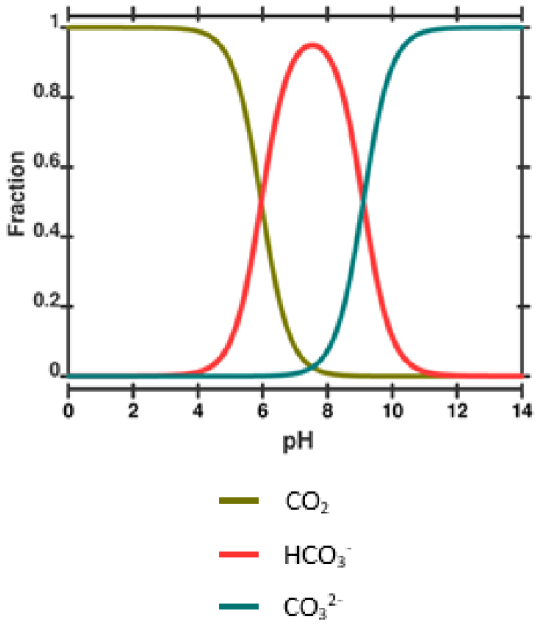

Figure 2.2: TIC equilibrium at 25 °C.

buffer system. At pH levels lower than 8.35 the weak acid H_2CO_3 and its conjugate base HCO_3^- are of importance, whereas HCO_3^- functions as weak acid with the conjugated base CO_3^{2-} at pH levels higher than 8.35. Within the acid-base pairs, the acid and conjugate base may react with one another, but this does not change their concentrations:

$$H_2CO_3(aq) + HCO_3^-(aq) \longrightarrow HCO_3^-(aq) + H_2CO_3(aq) \qquad \text{at pH} < 8.35 \qquad (2.19)$$

$$HCO_3^-(aq) + CO_3^{2-}(aq) \longrightarrow CO_3^{2-}(aq) + HCO_3^-(aq) \qquad \text{at pH} > 8.35 \qquad (2.20)$$

By definition, a weak acid only rarely dissociates in water losing a proton (H+). Likewise, a weak base rarely takes a proton from water.

In a buffer solution, pH only changes slightly when a strong base or strong acid is added. When a strong base is added, the weak acid will give up an H^+ in order to transform OH^- originating from the base into H_2O and the conjugate base:

$$H_2CO_3(aq) + OH^-(aq) \longrightarrow HCO_3^-(aq) + H_2O(l) \qquad \text{at pH} < 8.35 \qquad (2.21)$$

$$HCO_3^-(aq) + OH^-(aq) \longrightarrow CO_3^{2-}(aq) + H_2O(l) \qquad \text{at pH} > 8.35 \qquad (2.22)$$

When a strong acid is added, the weak base will react with H^+ originating from the acid to form the weak acid:

$$HCO_3^-(aq) + H^+(aq) \longrightarrow H_2CO_3(aq) \qquad \text{at pH} < 8.35 \qquad (2.23)$$

$$CO_3^{2-}(aq) + H^+(aq) \longrightarrow HCO_3^-(aq) \qquad \text{at pH} > 8.35 \qquad (2.24)$$

Because of the buffering effect of TAN in the form of NH_4HCO_3, a relatively large amount of base is needed to increase pH in a NH_4HCO_3 solution compared to solutions based on other ammonium salts such as ammonium chloride (NH_4Cl) and ammonium hydroxide (NH_4OH).

2.2 Membrane distillation driving force

2.2.1 Equilibrium vapor pressure calculation

Equilibrium vapor pressure or saturation vapor pressure is defined as the pressure exerted by a vapor in thermodynamic equilibrium with its condensed phases in a closed system. According to kinetic theory, liquids as well as gases are in constant agitation. In an open system, molecules evaporate from the surface of the liquid into the atmosphere above. In a closed system, however, particles return to the liquid phase in proportion to their concentration in the gaseous phase. Eventually a condition of equilibrium is established, in which the rate of return equals the rate of flight and the vapor is said to be saturated. When the temperature of a liquid increases, the kinetic energy of its molecules is enhanced. A higher fraction of molecules will turn to the vapor phase, resulting in a higher vapor pressure [37].

For a pure component, the (nonlinear) relationship between vapor pressure and temperature can be estimated using the Antoine equation (derived from the exponential Clausius-Clapeyron relation) [22,37]:

$$\log \mathrm{p}_i^* = \mathrm{A} - \frac{\mathrm{B}}{\mathrm{T} + \mathrm{C}} \tag{2.25}$$

In this equation, p_i^* is the vapor pressure of the pure component i and T temperature. Parameters A, B and C are component-specific parameters that depend on the volatility of the component; their exact values depend on the units used for p_i^* and T. The Antoine equation is based on the assumption of a temperature-independent heat of vaporization. As this is a valid assumption only over limited temperature ranges, different parameter sets are normally used for different temperature ranges.

In a mixture of components, the vapor pressure that a single component contributes to the total pressure in the system is called partial pressure. In a dilute solution, the vapor pressure of the component in large excess (the solvent) is proportional to its mole fraction. The constant of proportionality is the vapor pressure of the pure substance and Raoult's law can be used to calculate the vapor pressure of the solvent in the mixture:

$$\mathrm{p}_i = \mathrm{p}_i^* \cdot \mathrm{x}_i \tag{2.26}$$

In this equation, p_i is the partial vapor pressure of the component i, p_i^* is the vapor pressure of the pure component i and x_i is the mole fraction of the component i in the mixed solution.

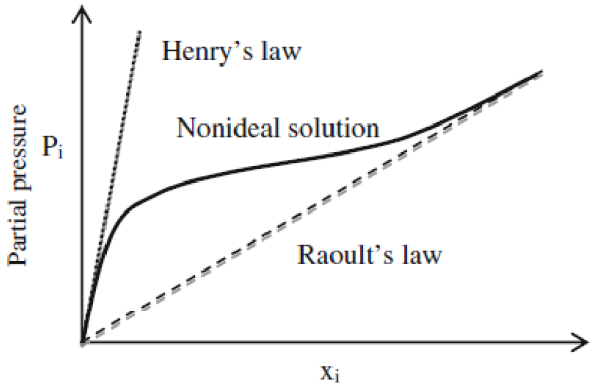

Figure 2.3: Applicability of Raoult's law and Henri's law [38].

The vapor pressure of the solute is also proportional to its mole fraction, but the constant of proportionality is different. In this case, the constant of proportionality is Henry's constant (K_H) and the vapor pressure can be calculated following Henry's law:

$$p_i = K_{H,i} \cdot x_i \tag{2.27}$$

It should be mentioned that a wide variety of units is used for K_H, depending on how the gas phase and liquid phase compositions are described. Moreover, Henry's law can be written in volatility form (measure of liquid phase composition equals Henry's constant times measure of gas phase) or in solubility form (measure of gas phase equals Henry's constant times measure of liquid phase composition), which are reciprocals of each other [46]. For any form, the dependency of K_H on temperature is described by the Van 't Hoff equation [36], which shows that gases indeed are less soluble at higher temperatures:

$$K_H(T) = K_H(T_{ref}) \cdot \exp\left[\frac{-\Delta H_{solv}}{R}\left(\frac{1}{T} - \frac{1}{T_{ref}}\right)\right] \tag{2.28}$$

Both Raoult's law and Henry's law assume ideal system behavior, with activity coefficients equal to unity. Interactions between gas molecules in a gas mixture are typically quite small; however, interactions in a liquid are very strong. Whereas a mixture of gases is ideal when there are no interactions between gas molecules, for a solution to be ideal the microscopic interactions between unlike molecules must be of the same magnitude as those between like molecules [41]. If deviations from the ideal system are small, Raoult's law and Henry's law are still valid. Basically, both are limit laws that apply at opposite ends of the composition range. Raoult's law is valid when the mole fraction $x_{textiti}$ approaches 1 (pure liquids), whereas Henry's law is valid when x_i approaches 0 (infinite dilution). This is depicted in Figure 2.3 [38].

Henry's constants can be adapted for non-ideal solutions [79,80]. In general, the solubility of a gas decreases with increasing salinity due to the effect of salting out (paragraph 2.1.2). Also Raoult's law can be adapted for non-ideal solutions, by incorporating a solvent activity coefficient that correcting for interactions between different molecules in the liquid phase [42]:

$$p_i = p_i^* \cdot x_i \cdot \gamma_i \tag{2.29}$$

In this equation, γ_i is the activity coefficient of the component i in the solution. Formulas to calculate the activity of H_2O in saline solutions are given in [77].

Once the components in a solution have reached equilibrium, the total vapor pressure (P) of the solution can be determined with Dalton's law of partial pressures:

$$P = p_A + p_B + ... + p_x \tag{2.30}$$

In this equation, p_i is the partial pressure of gas i. Dalton's law states that each gas exerts pressure independently of the other gases in the mixture, equal to the pressure that the gas would exert if no other gases would be present [37].

2.2.2 Ammonium bicarbonate feed solution in vacuum membrane distillation

In a VMD configuration, the total pressure on the permeate side is kept low by a (partial) vacuum induced by a vacuum pump. In the case of absolute vacuum, total pressure is 0 Pa and thus, also partial vapor pressures on the permeate side of the membrane are 0 Pa. Absolute vacuum has rarely been applied in MD research; usually, a partial vacuum is applied [11,22,25-30,40]. In that case, the total pressure on the permeate side of the membrane will be occupied by partial vapor pressures of evaporated components.

It should be emphasized that in MD, only gaseous components can be removed from a feed solution. Three of the components in the equilibria described in paragraph 2.1.2 can vaporize from a

NH_4HCO_3 solution, namely H_2O, NH_3 and CO_2. Their vapor pressures (p_{H_2O}, p_{NH_3} and p_{CO_2}, respectively) under applied conditions can be calculated following Raoult's law for H_2O and Henry's law for NH_3 and CO_2, with the laws as explained in paragraph 2.2.1. Figure 2.4 shows the vapor pressures in a system in which a NH_4HCO_3 feed solution and a VMD configuration are combined. For the creation of a high quality SOFC fuel gas, NH_3 transport should be maximized while H_2O and CO_2 transport should be minimized. Hence, the driving force for NH_3 transport ($p_{NH_3,feed} - p_{NH_3,permeate}$) should be maximized while the driving forces for H_2O and CO_2 transport ($p_{H_2O,feed} - p_{H_2O,permeate}$ and $p_{CO_2,feed} - p_{CO_2,permeate}$, respectively) should be minimized.

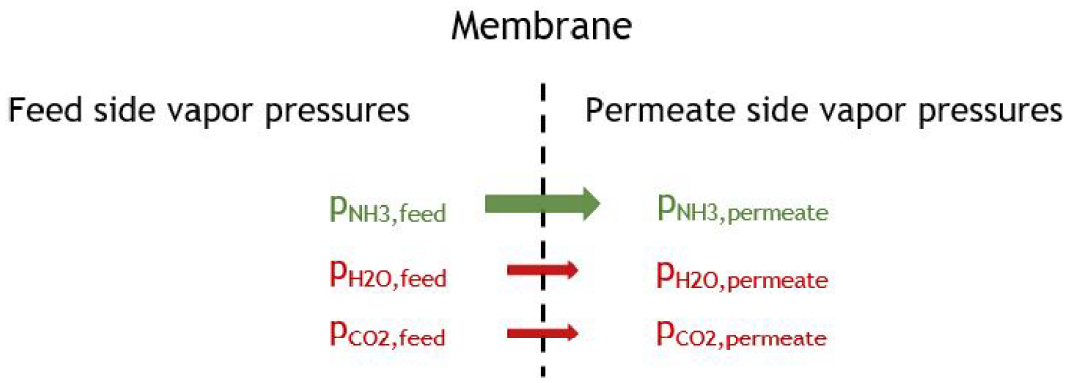

Figure 2.4: Vapor pressures on feed and permeate side in VMD for a NH_4HCO_3 solution.

2.3 Mass transfer and mass transfer resistance

2.3.1 Mass transfer coefficient

As explained in paragraph 2.2, the driving force for mass transfer in MD is the difference in vapor pressure over membrane pore entrances. Mass transfer in VMD takes place in three steps [12]:

1. Mass transfer from bulk feed to the feed side membrane surface;
2. Mass transfer through membrane pores;
3. Mass transfer from membrane pores into the permeate phase.

In all three steps, a resistance to mass transfer occurs that influences the vapor pressure at the feed or permeate side of the membrane and thereby the vapor pressure difference over the membrane pores. In literature, often an overall mass transfer coefficient K_{OV} (m/s) is adopted for the volatile component to be transported through the membrane. This K_{OV} consists of three separate mass transfer coefficients and can be expressed by a resistance in series model [12]:

$$\frac{1}{K_{OV}} = \frac{1}{K_f} + \frac{1}{K_m} + \frac{1}{K_p} \tag{2.31}$$

In this equation, K_f, K_m and K_p are the feed, membrane and permeate mass transfer coefficients, respectively, corresponding to the three steps of mass transfer. Mass transfer resistance at the permeate side is usually considered negligible in VMD configurations due to the low downstream pressures [12]. In that case, the overall mass transfer resistance in VMD modules reduces to the first two terms of the right-hand side of the expression.

K_{OV} can be determined using the following equation:

$$K_{OV} = \frac{V}{At} \cdot \ln\left(\frac{C_0}{C_t}\right) \tag{2.32}$$

In this equation, V is the initial liquid volume of the feed solution, A the membrane area and C_0 and C_t are the concentration of the volatile component (e.g. NH_3) at start-up and at a time t, respectively. K_{OV} is determined from the slope of the graph of $\ln(C_0/C_t)$ over time (obtained experimentally) and is normally expressed in m/s, with V in m^3, A in m^2, t in s and C_0 and C_t in mol/m^3 or g/m^3. The formula is derived from the integration of combined expressions for flux and the unsteady state mass balance of the volatile component in the feed solution. The expression for flux assumes ideal behavior following Henry's law for the volatile component in the feed solution and negligible partial pressures of both the volatile component and water on the permeate side of the membrane [50].

Within MD literature, the dusty gas model is usually applied to describe the mass transfer across membrane pores. According to the dusty gas model, transmembrane fluxes in MD can be dominated by a molecular diffusion mechanism, a Poiseuille flow mechanism, a Knudsen diffusion mechanism or a combination of any of them [12,17]. When VMD operates at total pressures below the vapor pressure of water, only trace amounts of air exist in the membrane pores and mass transfer resistance caused by molecule-molecule collision can be neglected. K_m in Equation 2.32 can then be expressed as a combination of Knudsen and Poiseuille flow mechanisms [12]:

$$K_m = \frac{8}{3}\frac{\epsilon r}{\tau\delta}\sqrt{\frac{1}{2\pi RTM}} + \frac{\epsilon r^2}{\tau\delta}\frac{1}{8\mu}\frac{P_m}{RT} \tag{2.33}$$

In this expression, ϵ is the membrane porosity, τ the pore tortuosity, δ the membrane thickness, r the average pore radius, P_m the average pressure within the membrane pores, R the universal gas constant, M the molecular weight of the transported molecules, μ its viscosity and T temperature. It should be noted that P_m and μ are functions of T. When small pore sizes and low permeate pressures are employed, as is often the case in VMD configurations, Poiseuille flow may sometimes be neglected. The membrane mass transfer coefficient can then be described by the Knudsen mechanism only, which is the first term of the right-hand side of Equation 2.33 [12,17]. As membrane manufacturers often do not supply (all) data on membrane morphology, membrane characteristics usually have to be determined experimentally for calculation of K_m. A qualitative description of membrane characteristics and their influence on MD is given in paragraph 2.3.2.

K_f is influenced by temperature and concentration boundary layers adjacent to the membrane surface (explained further in paragraph 2.3.3). Sometimes a Sherwood correlation is used to estimate K_f [17]; this is not further elaborated upon in this thesis. Mostly, K_f is derived from the experimentally determined K_{OV} and the calculated K_m using Equation 2.32 (under the assumption that K_p is negligible) [11,12].

The K_{OV} used in literature might be convenient when removal of volatile components from a feed solution is studied; however, it does not directly relate the MD driving force of vapor pressure differences to mass transfer. A more convenient expression for the application of MD for the production of an SOFC fuel gas links flux (J) to the vapor pressure difference between the feed bulk and permeate bulk directly by means of a global mass transfer coefficient (K_g) [81,82]:

$$J_i = K_{g,i}(p_{i,\text{feed}} - p_{i,\text{permeate}}) \tag{2.34}$$

In literature, K_g is also indicated as C, B or another symbol. K_g includes the resistances of all three mass transfer steps. When units of Pa ($kg/m/s^2$) is used for p and $kg/m^2/s$ for J, K_g has units of s/m. J increases with increasing K_g for a certain vapor pressure difference. When a vapor pressure difference has been calculated and/or determined from simulations, expected J can be calculated if the K_g is known for the considered membrane system and settings. K_g must be determined for

each volatile component individually.

K_g and K_{OV} can be related to each other when the same assumption of negligible partial pressures on the permeate side of the membrane is made in Equation 2.34 as has been made to derive Equation 2.34. In that case, K_g and K_{OV} are related through Henry's law constant:

$$K_g = \frac{K_{OV}}{K_H} \tag{2.35}$$

With a solubility form of Henry's law ($p_i = K_{H,i} \cdot C_i$; where C_i is the concentration of volatile component i in the feed solution), units of kg/m^3 for C and units of Pa ($kg/m/s^2$) for p, K_H has units of m^2/s^2. It should be noted that it must always be verified whether or not permeate side pressures may be considered negligible. K_g and K_{OV} show opposite trends with increasing temperature. Whereas the influence of temperature on vapor pressure is included in K_{OV}, it is included as a driving force in Equation 2.34 directly (and not in K_g). Due to the (exponential) increase of vapor pressure with temperature, K_{OV} increases with increasing temperature [11]. K_g, on the other hand, decreases due to increased resistances at higher temperatures (explained further in paragraph 2.3.3).

2.3.2 Membrane characteristics

The membranes applied in MD are usually (hydrophilic) membranes developed for microfiltration purposes, prepared using polymers to give them a hydrophobic character [12,17]. Membrane characteristics that affect the MD process are described qualitatively [12,17,48]:

- *Hydrophobicity:*
  Membranes used in MD should exhibit strong hydrophobicity to prevent the entry of liquid into the pores. Hydrophobicity of a material can be determined by measurement of the contact angle between the surface of the wetted solid and a line tangent to the curved surface of the drop at the point of three-phase contact (Figure 2.5). The greater the contact angle, the stronger the hydrophobicity of the material. Due to their strong hydrophobicity, the most commonly applied materials in MD membrane preparation are (in descending order of hydrophobicity) polytetrafluoroethylene (PTFE), polyvinylidene fluoride (PVDF) and polypropylene (PP).

- *Thickness:*
  Membrane thickness plays a significant role in the resistance to mass transfer, but also in conductive heat transfer through the membrane. Whereas desired mass transfer is inversely proportional to the thickness and a thin membrane would be preferred, undesired heat loss is also inversely proportional to membrane thickness due to which a thick membrane would be favorable. As conductive heat losses are negligible in VMD (elaborated further upon in paragraph 2.6.1), preference would be given to a thin membrane in VMD configurations.

- *Porosity:*
  Membrane porosity is an important parameter positively affecting MD mass transport, as evaporation is a surface phenomenon. High porosity also results in lower conductive heat losses since the conductive heat transfer coefficient of gases entrapped within membrane pores is an order of magnitude smaller than that of the hydrophobic polymeric membrane material. This is an additional advantage in other configurations than VMD.

- *Pore size:*
  Large pore size is favorable in terms of mass transport, but disadvantageous in relation to pore wettability. As the applied (partial) vacuum pressure results in a large transmembrane pressure, the risk of pore wetting is especially high in VMD configuration. A liquid entry pressure (LEP) can be defined that should not be exceeded by the transmembrane pressure. Furthermore, it should be mentioned that membranes employed in MD exhibit a pore size distribution rather than a uniform pore size, which complicates predictions of the extent in which mass and heat transfer mechanisms will occur.

- *Tortuosity:*
  Generally, pores do not go straight across a membrane. Diffusing molecules must move along tortuous paths (Figure 2.6). Pore tortuosity is defined as the average length of pores compared to membrane thickness. Tortuosity negatively affects mass transfer, as it imposes a resistance.

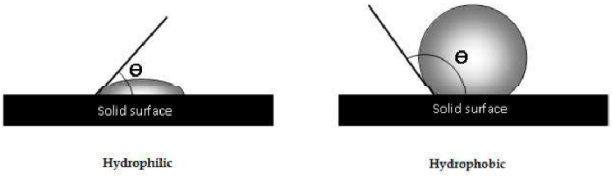

Figure 2.5: Contact angle [48].

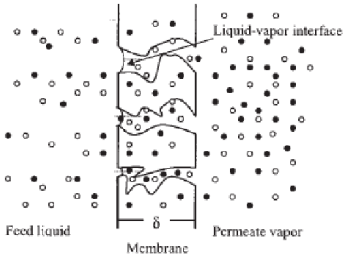

Figure 2.6: Tortuosity [49].

2.3.3 Polarization effects and hydrodynamic conditions

Temperature polarization

In VMD, heat transfer takes place in two steps [12]:

1. Heat used for vaporization at the feed side membrane surface;
2. Heat transfer from the feed bulk to the feed side membrane surface.

Figure 2.7 shows that the bulk feed temperature (T_{fb}) is gradually decreased across a feed side thermal boundary layer of thickness (δ_{ft}) to a temperature at the feed side membrane surface (T_{fm}). This phenomenon is called temperature polarization and occurs when heat losses through vaporization at the membrane surface (step 1) happen at a higher rate than heat transfer from the higher temperature feed bulk solution to the lower temperature region at the membrane surface (step 2). Temperature polarization negatively affects the driving force for mass transport, as a decreased temperature at the membrane surface leads to lower vapor pressure differences over the membrane [12,17].

In other MD configurations than VMD, extra steps in heat transfer occur in the form of heat loss across the membrane material and pores and heat transfer from the membrane surface to the permeate solution across a permeate side thermal boundary layer. In VMD, these steps in heat transfer are considered negligible due to the existence of low partial pressure at the permeate side of the membrane. It should be noted that heat transfer in VMD is not fully understood yet and that further research in this area is required [12].

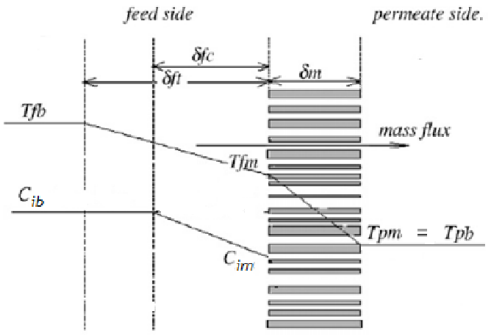

Figure 2.7: Temperature and concentration polarizations in VMD [12].

Concentration polarization

A mentioned in paragraph 2.3.1 already, mass transport in VMD takes place in three steps (that are repeated here for convenience) [12]:

1. Mass transfer from bulk feed to the feed side membrane surface;
2. Mass transfer through membrane pores;
3. Mass transfer from membrane pores into the permeate phase.

Considering the removal of volatile compounds from aqueous solutions (e.g. NH_3 in the production of an SOFC fuel gas), a feed side concentration boundary layer of thickness (δ_{fc}) may exist composed of the solvent (e.g. H_2O). The concentration of a component i decreases across the δ_{fc} from $C_{i,\mathrm{b}}$ in the bulk feed phase to $C_{i,\mathrm{m}}$ at the membrane surface (Figure 2.7). This phenomenon is called concentration polarization and is due to the removal of volatile compounds at the membrane surface (step 2) occurring at a higher rate than mass transfer from the higher concentration feed bulk solution to the lower concentration region at the membrane surface (step 1). Concentration polarization negatively affects the driving force for mass transport of a component i, as a decreased concentration at the membrane surface leads to a lower vapor pressure difference over the membrane.

When a solvent containing non-volatile solutes is considered, another type of concentration polarization takes place. In that case, a concentration polarization layer consisting of solutes may occur. The vapor pressure of the solvent at the membrane surface drops, as the activity and mole fraction of the solvent decrease (according to Raoult's law, as described in paragraph 2.3). This negatively affects mass transfer of the solvent [12]. Both types of concentration polarization can occur simultaneously in a solution.

Vapor pressure increases exponentially with temperature (paragraph 2.2.1), resulting in higher transmembrane fluxes at higher temperatures. Also, polarization effects increase with temperature [17]; apparently, heat losses due to vaporization increase to a larger extent than heat transfer from the feed bulk to the feed side membrane surface. The influence of temperature polarization is dominant over the influence of concentration polarization, especially at higher temperatures [17].

Various empirical heat and mass transfer correlations have been proposed for the prediction and modelling of MD transmembrane fluxes. However, their applicability is questionable since MD systems are generally different from the test systems used to determine these correlations. Moreover, temperature and concentration variations along the length of a membrane module are not taken into account in MD modelling with empirical correlations [12].

Flow conditions in spacer-filled flow channels

The thicknesses δ_{ft} and δ_{fc} of the polarization boundary layers are functions of fluid properties and operating conditions. Optimum hydrodynamic conditions of unsteady or turbulent flow diminish polarization effects, stimulating gas transport through the MD membrane [12].

The dimensionless Reynolds number (Re) can be used to determine whether the flow in a channel is laminar, transient or turbulent [46]:

$$\mathrm{Re} = \frac{\mathrm{uD}}{\nu} \tag{2.36}$$

In this equation, u and ν are the velocity (in m/s) and the kinematic viscosity (in m^2/s) of the stream passing through the flow channel, respectively, and D is a characteristic length for the flow channel in m. The flow in a channel becomes more unsteady with increasing Re. In spacer-filled flow channels, D can be represented by a hydraulic diameter (d_H) [43-45]:

$$d_H = \frac{4\varepsilon}{\frac{2}{h} + 4(1-\varepsilon)/d_f} \tag{2.37}$$

In this equation, ε is the dimensionless void volume fraction in the channel, h the channel or spacer height in m and d_f the diameter of spacer filaments in m. As the formula shows, d_H is dependent on the dimensions of both the flow channel and the spacer material. The derivation of Equation 2.37 is presented in Appendix B1.

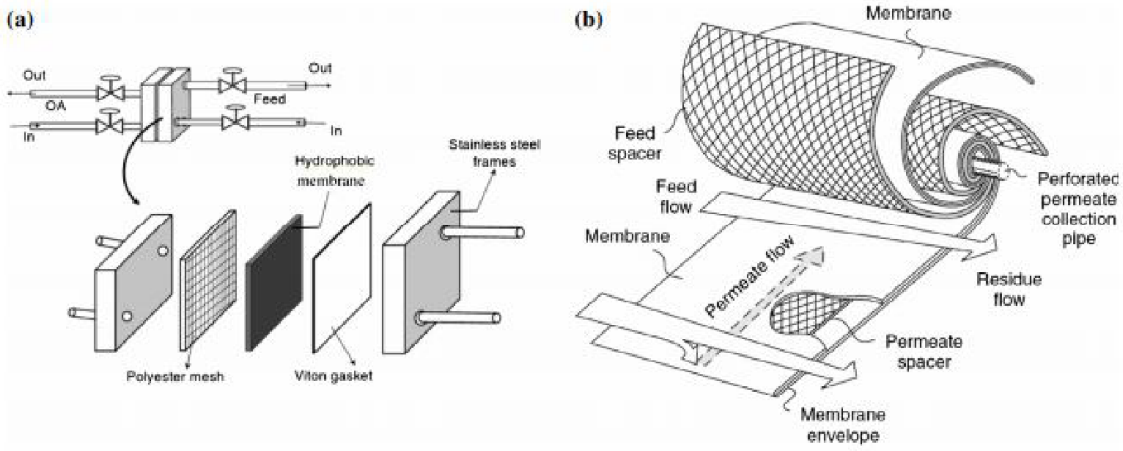

Figure 2.8: Possible flat-sheet MD configurations with use of spacers on lab scale (a) and commercial scale (b).

In flat-sheet MD configurations, membrane spacers can be used to reduce the void volume in flow channels (Figure 2.8). This raises effective velocities and results in lower required Re values to achieve unsteady or turbulent flow [45]. According to literature findings, the flow characteristics in spacer-filled channels show that flow is steady for $\mathrm{Re} < 300$, increasingly unsteady from $\mathrm{Re} = 350$ onwards and at the onset of turbulent flow at $\mathrm{Re} = 1000$ (Figure 2.9) [43]. In comparison, Re values higher than 2000 are required to achieve turbulent flow in similar channels without application of spacer material [11].

When the d_H for a MD flow channel has been calculated and a value of Re has been chosen based on the desired degree of turbulence, Equation 2.36 can be rewritten in order to determine the required cross flow velocity of the feed solution:

$$u_{required} = \frac{\nu \cdot \mathrm{Re}}{\mathrm{D}} = \frac{\nu \cdot \mathrm{Re}}{d_H} \tag{2.38}$$

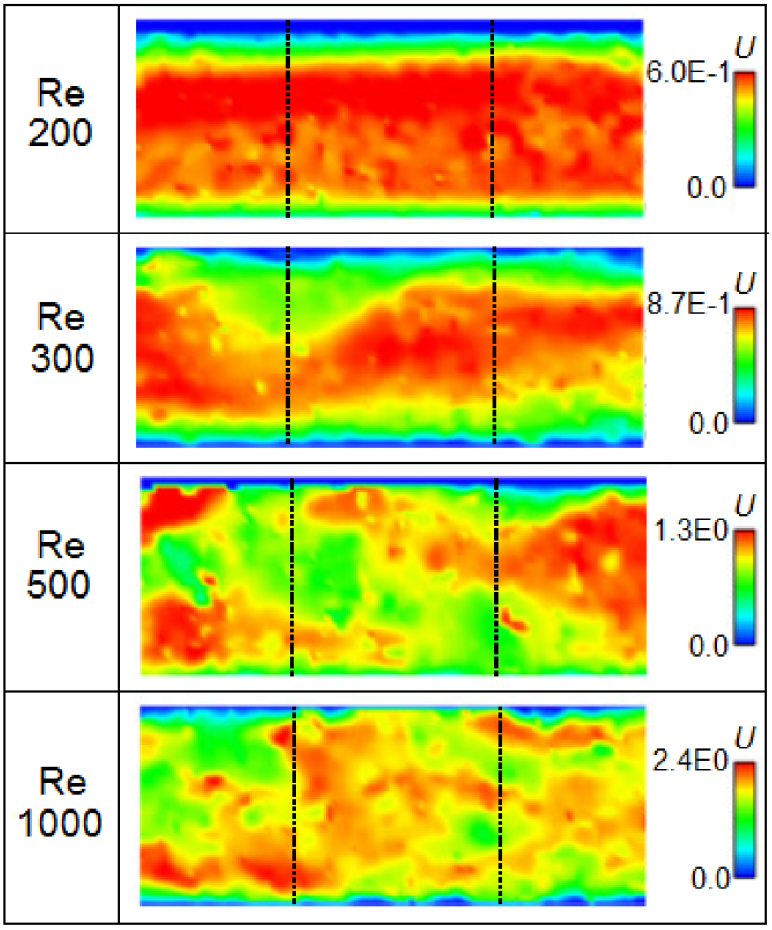

Figure 2.9: Typical instantaneous velocity fields in spacer-filled channels by optical methods of flow visualization (top view) for values of Re in the range from 200 to 1000 [43].

Chapter 3

Selection of experimental test conditions

3.1 Literature concentration factors for ammonia concentration selection

In literature, the effectiveness of the separation of dissolved gases from feed solutions is reported by a parameter named separation factor or selectivity (α) [12,17, 21, 25]:

$$\alpha = \frac{\mathrm{x}_{i,\mathrm{permeate}}/(1-\mathrm{x}_{i,\mathrm{permeate}})}{\mathrm{x}_{i,\mathrm{feed}}/(1-\mathrm{x}_{i,\mathrm{feed}})} \tag{3.1}$$

In this equation, $\mathrm{x}_{i,\mathrm{permeate}}$ and $\mathrm{x}_{i,\mathrm{feed}}$ are the mass fractions of the target component i (i.e. NH_3) in permeate and feed, respectively. When $\mathrm{x}_{i,\mathrm{permeate}}$ and $\mathrm{x}_{i,\mathrm{feed}}$ are close to zero, (α) approximates the concentration factor (β):

$$\beta = \frac{\mathrm{C}_{i,\mathrm{permeate}}}{\mathrm{C}_{i,\mathrm{feed}}} \tag{3.2}$$

In this equation, $\mathrm{C}_{i,\mathrm{permeate}}$ and $\mathrm{C}_{i,\mathrm{feed}}$ are the concentrations of the target component i in the permeate and feed, respectively. For the removal of NH_3 from a watery solution by means of VMD, α values of 3–11 have been reported for feed solutions with up to 2.1 mass percent NH_3 (corresponding to about 21 g TAN/L) [17]. Considering these concentrations as close to zero, this would mean that $\mathrm{C}_{i,\mathrm{permeate}}$ was 3 to 11 times the $\mathrm{C}_{i,\mathrm{feed}}$ in the studies presented in literature. For reject water (1.5 g TAN/L) and urine (6 g TAN/L), this can be translated to permeate concentrations of 4.5 to 16.5 g TAN/L and 18 to 66 g TAN/L, respectively, or to permeate qualities of about 0.45 to 1.65 m% NH_3 and 1.8 to 6.6 m% NH_3.

As can be concluded from Chapter 2, feed solution characteristics, membrane properties and test conditions all have an influence on transmembrane fluxes. Therefore, α depends on them as well. Nonetheless, the α values obtained in studies presented in literature can give an impression of what can approximately be expected in any MD system for the production of an NH_3 gas. To give an impression of the test conditions applied in the studies; temperatures were 42 to 56 °C and partial vacuum pressures 3 to 10 kPa. As NH_3 has a lower boiling point than H_2O (−33 °C versus 100 °C) and hence is more volatile, it is expected that at lower temperatures even higher concentration factors can be obtained.

As the minimum MD permeate quality required for the application of the permeate gas as SOFC fuel is 5–10 m% NH_3 (paragraph 1.3.3), it is expected that a concentration step is inevitable for the production of an SOFC NH_3 fuel gas from reject water or urine. A concentration step is topic of research in one of the tracks of the *From pollutant to power* project (paragraph 1.1.3) and the possibility of its inclusion is assumed (paragraph 1.3.3). At the moment, electrodialysis (ED) is considered as a promising concentration method within the *From pollutant to power* project with respect to energy usage. With achievable concentration factors of three to four [51-53], the ED process as a preceding step to MD is expected to give a maximum feed TAN concentration of about 20 g/L for a single stage of ED (with urine TAN concentration as initial concentration). That could suffice for the production of an SOFC ammonia fuel gas, when the concentration factors known from literature are adopted. 20 g TAN/L was selected as the highest concentration to test in laboratory scale experiments. To prove the need of a concentration step, the lowest considered influent concentration of 1.5 g TAN/L (reject water) was selected as the lowest concentration to test in laboratory scale experiments. To see whether a trend could be observed, a third concentration of 12 g TAN/L was included as well. This concentration could for example be obtained by applying one ED stage for urine or multiple stages of ED for reject water.

3.2 PHREEQC simulations for pH selection

Geochemical models can easily take electrostatic shielding effects and the formation of aqueous complexes (paragraph 2.1.2) into account in equilibrium calculations [39,75]. The code PHREEQC was used in this master thesis research for simulations of system equilibrium in order to estimate

the TAN equilibrium and vapor pressures in MD feed solutions. Simulations were carried out for the selected experimental concentrations of 1.5, 12 and 20 g TAN/L.

In PHREEQC, equilibrium calculations are not related to kinetics. The database *Amm.dat* was used to prevent kinetically slow redox reactions related to oxidation states of N from leading to unrealistic results for water treatment processes with short residence times. In this database, N_2 and NH_4^+ are defined as inert substances [54]. Even though kinetics have a predominant role in water treatment, a considerable part of the reactions described by equilibrium will actually develop during treatment processes [54].

3.2.1 Total ammonia nitrogen equilibrium simulations

The TAN equilibrium was determined by PHREEQC simulations as the molar ratio NH_3/TAN over pH for temperatures from 20 to 70 °C. The feed solutions defined for simulation contained TAN in the form of NH_4HCO_3. To correct the pH of the introduced solution to the desired pH, NaOH or HCl was added to increase or decrease pH, respectively.

Simulation results for a 1.5 g TAN/L solution are presented in Figure 3.1. As expected, the ratio NH_3/TAN increases with increasing pH and with increasing temperature (paragraph 2.1.2). As TAN can only be removed in MD as NH_3, high values of pH and temperature are favorable in terms of the TAN equilibrium. Simulation results for feed solutions with 12 and 20 g TAN/L are presented in Appendix C. Comparing the graphs for the different TAN concentrations, it can be seen that a higher concentration leads to a lower NH_3 fraction. This effect is more explicit at lower pH values (the closer to pH 7, the lower the NH_3 fraction for a certain temperature) and lower temperatures (the closer to 20 °C, the lower the NH_3 fraction for a certain pH value). It is explained by a combination of the shift in the TAN equilibrium in the direction of NH_3 at increasing pH and temperature (paragraph 2.1.2) and higher ionic strengths at higher TAN concentrations. Not only does ionic strength increase by addition of more NH_4HCO_3 to obtain higher TAN concentrations, but also by the higher amount of base or acid required for pH correction due to a higher buffering effect (paragraph 2.1.2) at higher HCO_3^- concentrations (resulted from a larger amount of NH_4HCO_3 in solution). The increased ionic strength results in a lower NH_4^+ reactivity . The largest differences in NH_3/TAN ratio in the simulation results of the TAN equilibrium for the different feed solution TAN concentrations occur at pH 7 and 20 °C. They amount to decreases of 35 and 46% for 12 and 20 g TAN/L feed solutions, respectively, compared to the NH_3/TAN ratio simulated for a 1.5 g TAN/L solution. From pH 11 on, deviations from the NH_3/TAN ratio in the 1.5 g TAN/L feed solution are less than 5% for all temperatures and for both 12 and 20 g TAN/L feed solutions.

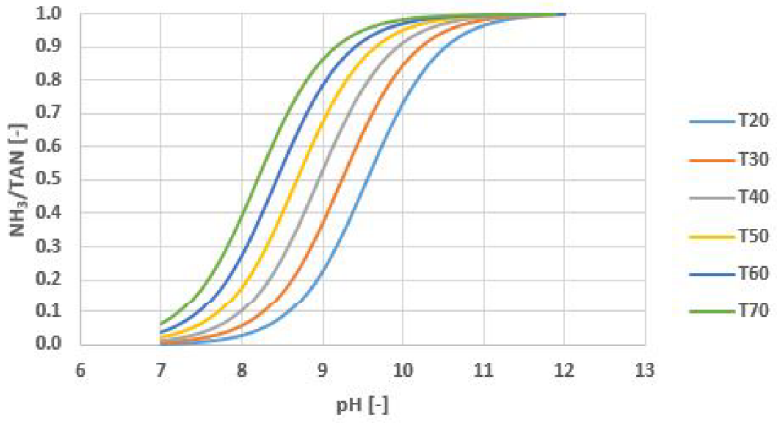

Figure 3.1: TAN equilibrium for a 1.5 g TAN/L NH_4HCO_3 feed solution (PHREEQC simulation).

PHREEQC simulation results regarding the TAN equilibrium were verified with manual calculations (Appendix C3).

3.2.2 Vapor pressure simulations

It was recognized in paragraph 2.4 that three components can vaporize from a NH_4HCO_3 solution, namely H_2O, NH_3 and CO_2. The vapor pressures of these components were obtained by PHREEQC simulations.

In PHREEQC, calculated equilibrium vapor pressures are presented in the form of a saturation index (SI) for each gaseous component *i*. The PHREEQC SI output can be recalculated to a vapor pressure for each gas component (p_i) in units of atm:

$$p_i = \frac{10^{SI_i}}{\varphi} \tag{3.3}$$

In this equation, φ is a fugacity coefficient that corrects for gas non-ideality by taking interactive forces between molecules into account. When the prevailing pressure is below 10 atm, this correction can be neglected by assuming $\varphi = 1$ [39,40]. As 1 atm equals 101325 Pa, the p_i in atm resulting from Equation 3.3 can be converted to a p_i in Pa by multiplication with the factor 101325 Pa/atm.

Vapor pressures recalculated from PHREEQC SI values for H_2O, NH_3 and CO_2 in feed solutions with TAN concentrations of 1.5, 12 and 20 g/L are presented in Appendix D. The plots show p_{H_2O}, p_{NH_3} and p_{CO_2} over temperature for pH values from 7 to 12. Again, TAN concentrations for simulation were defined by NH_4HCO_3 solution and NaOH and HCl were added for pH corrections. All p_{H_2O}, p_{NH_3} and p_{CO_2} increase exponentially with temperature when the concerned volatile component is present in the feed solution, which is due to the temperature-vapor pressure relations according to the Antoine equation and the Van 't Hoff equation (paragraph 2.2.1).

Considering the graphs describing p_{H_2O} for the different TAN concentrations, it can be concluded that the p_{H_2O} is not dependent on pH. The largest deviation in p_{H_2O} occurs in a 20 g TAN/L feed solution and amounts to a decrease of 2.7% at 70 °C for pH 12 compared to pH 7. A small influence of ionic strength is shown as a decrease in p_{H_2O} for increasing TAN concentration; maximum deviations are decreases of 3.4 and 5.7% in p_{H_2O} at 70 °C in 12 and 20 g TAN/L feed solutions compared to a 1.5 g TAN/L feed solution, respectively. The deviations are explained by a combination of decreases in H_2O mole fraction in Raoult's law for p_{H_2O} calculation (paragraph 2.2.1) and in H_2O activity (paragraph 2.1.2.) due to a higher ionic strength at higher feed solution TAN concentrations.

Considering the graphs describing p_{NH_3} for the different TAN concentrations, it can be concluded that p_{NH_3} is very much dependent on the feed solution TAN concentration. This can be explained by the usage of Henry's law for p_{NH_3} caluculations, resulting in higher vapor pressures at higher NH_3 concentrations or mole fractions (paragraph 2.2.1. The p_{NH_3} is also dependent on pH up to a pH of about 11, which is attributed to the relation between TAN equilibrium and pH (paragraph 2.1.2).

Considering the graphs describing p_{CO_2} for the different TAN concentrations, it can be concluded that also p_{CO_2} is very much dependent on the feed solution TAN concentration. This can be explained by the usage of Henry's law for p_{CO_2} calculations, resulting in higher vapor pressures at higher CO_2 concentrations or mole fractions (paragraph 2.2.1). CO_2 concentrations increase with TAN concentration, as TAN is added in the form of NH_4HCO_3 that dissociates into equal molar quantities of NH_4^+ and HCO_3^-. CO_2 originates from the HCO_3^- part of the NH_4HCO_3 salt according to the TIC equilibrium (paragraph 2.1.2). Moreover, it can be see that CO_2 concentration is highly dependent on pH. This too is attributed to the TIC equilibrium, in which CO_2 is only present at pH values lower than about 8 (the exact pH value depending on temperature and ionic

strength, that influence the TIC equilibrium) (paragraph 2.1.2).

Comparing the absolute values of p_{H_2O}, p_{NH_3} and p_{CO_2}, it can be seen that for all three concentrations p_{CO_2} is dominant over p_{H_2O} and p_{NH_3} at low pH values of 7 and 8. Whereas at pH 9 it still contributes to about 50% of the total vapor pressure (P) at low temperatures and high TAN concentrations, it contributes less than 2% to P for all temperatures and concentrations at pH 10 and its contribution decreases even further with pH increase above pH 10. Moreover, it can be concluded that p_{H_2O} is always larger than p_{NH_3} for the selected feed solution concentrations of 1.5, 12 and 20 g TAN/L.

Results from PHREEQC simulations regarding vapor pressures were verified with literature data and manual calculations for H_2O and NH_4OH solutions, respectively (Appendix C3).

3.2.3 Selection of experimental pH

From the vapor pressures of H_2O, NH_3 and CO_2 determined from PHREEQC simulations (paragraph 3.2.2), it was concluded that the minimum pH value for VMD for the production of an SOFC fuel gas should be 10. At pH values lower than 10, p_{CO_2} is larger than p_{H_2O} and p_{NH_3} to an extent at which it is expected to drastically and negatively affect permeate quality.

For pH values higher than 10, the TAN equilibrium is shifted in the direction of NH_3 for all three of the selected TAN concentrations. As the ratio NH_3/TAN depends on TAN concentration and temperature as well (paragraph 2.1.2), the extent to which the shift towards NH_3 establishes at pH 10 varies. It varies from NH_3/TAN ratios of 0.73-0.98 for a 1.5 g TAN/L feed solution, of 0.62-0.98 for a 12 g TAN/L feed solution and of 0.56-0.97 for a 20 g TAN/L feed solution for temperatures ranging from 20 to 70 °C (Appendix C1).

The unadjusted pH of NH_4HCO_3 solutions varies from 7.2 at 70 °C to 7.8 at 20 °C for the selected TAN concentrations and thus should be increased to obtain a pH value of 10. Increase of pH could be realized through addition of a base; however, chemical additions are not desired in the view of the *From pollutant to power* project. When base addition is used for pH increase, applied pH values should be high enough to produce a permeate fuel on which an SOFC can run but as low as possible to minimize chemical additions. Another method to increase pH is the application of bipolar membranes in an ED concentration step (Appendix D) [84]. Internal results of the *From pollutant to power* project up to now show a maximum obtained pH value of 10 (Appendix E).

Based on the above considerations, pH 10 was considered as most realistic value to apply and was therefore selected for laboratory scale experiments.

3.3 PHREEQC simulations for temperature range selection

In Figure 3.2, p_{H_2O} and p_{NH_3} at pH 10 are shown in one figure to show the remark made in paragraph 3.2.2 that p_{NH_3} is lower than p_{H_2O} for the selected concentrations and all temperatures from 20 to 70 °C. In Figure 3.3, the ratio p_{NH_3} over total vapor pressure (p_{NH_3}/P) is shown to give a first estimate of the relative driving forces and hence permeate quality that might be obtained with MD. A 20 g TAN/L feed solution has been taken as example, but simulation results for 1.5 and 12 g TAN/L feed solutions show similar trends. Figure 3.3 shows that the ratio p_{NH_3}/P for pH 10 increases to a maximum at temperatures from 35 to 40 °C and decreases with temperature for temperatures higher than 40 °C. That the ratio p_{NH_3}/P is lower at temperatures below 30 °C is attributed to the TAN equilibrium, which shows a lower NH_3/TAN ratio at lower temperatures in the temperature range of 20 to 70 °C (Figure 3.4). In order to show that this is indeed the cause, p_{NH_3}/P for pH values of 11 and 12 is plotted as well in Figure 21. At pH 11 and 12 the ratio NH_3/TAN is practically equal to 1 even at low temperatures and indeed, the ratio p_{NH_3}/P shows a decrease with temperature over the entire temperature range of 20 to 70 °C. It should be

noted that permeate partial pressures and mass transfer coefficients of H_2O and NH_3 (Equation 2.34) are not included in the curves presented in Figure 20. Therefore, this plot cannot be used directly for the prediction of permeate fuel gas quality. Permeate partial pressures depend on the applied (partial) vacuum pressure and on mass transfer resistances and cannot be predicted without knowledge of transmembrane fluxes.

The decreasing trend of the ratio p_{NH_3}/P with increasing temperature for a NH_3/TAN ratio approaching 1 is caused by the larger increase of p_{H_2O} compared to the increase of p_{NH_3}. As a high m% NH3 in the permeate gas is desired, it is expected that even though increased temperatures are beneficial in terms of vapor pressures (and as a result, in terms of permeate quantity), they might not be favorable in terms of permeate quality. Working at lower temperatures might be preferred as well in terms of energy. In VMD processes, heating accounts for the largest part of the total energy requirement [11]. As the overall goal of the *From pollutant to power* project is to create a net energy producing system, energy consumption for NH_3 gas production is considered an important parameter.

Based on the previous, a temperature range of 25 °C (room temperature) to 55 °C was selected for laboratory scale experiments. Temperatures usually applied in MD applications are generally higher than 45 °C [12].

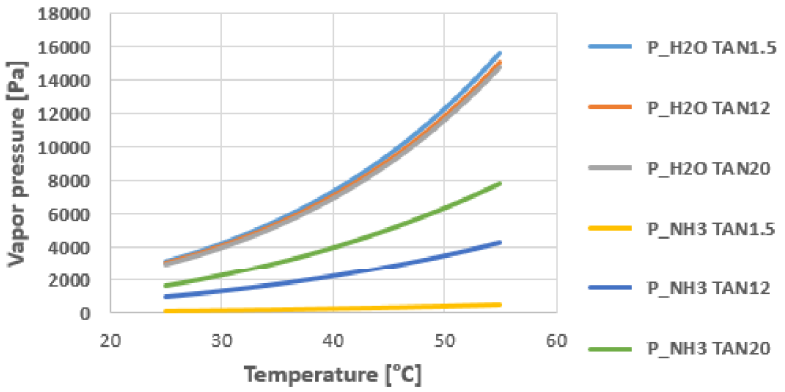

Figure 3.2: H_2O and NH_3 vapor pressures for the selected concentrations and pH 10.

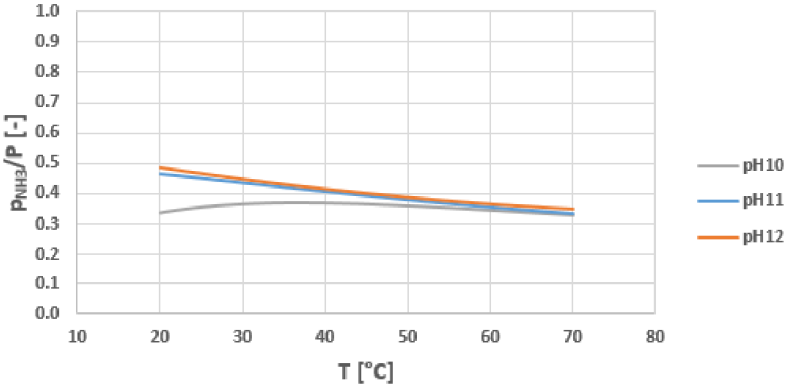

Figure 3.3: p_{NH_3}/P for a 20 g TAN/L solution and pH values of 10, 11 and 12.

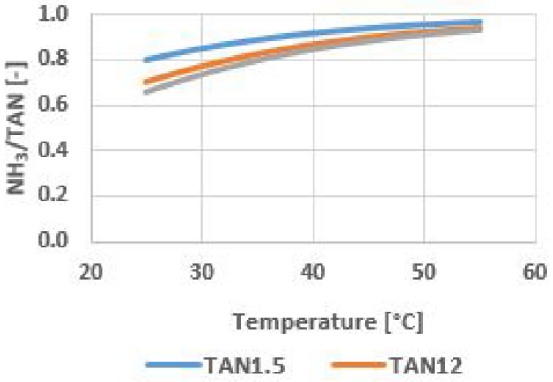

Figure 3.4: TAN equilibrium for pH 10, 11 and 12.

3.4 Summary of selected experimental conditions

The selected conditions for laboratory scale experiments are summarized in Table 3.1. Abbreviations of the test conditions that will be used for refering in the next chapters of this report are included as well.

Table 3.1: Overview of the combinations of selected test conditions for experiments and how they can be referred to.

pH10	25 °C	35 °C	45 °C	55 °C
1.5 g TAN/L	TAN1.5_T25	TAN1.5_T35	TAN1.5_T45	TAN1.5_T55
12 g TAN/L	TAN12_T25	TAN12_T35	TAN12_T45	TAN12_T55
20 g TAN/L	TAN20_T25	TAN20_T35	TAN20_T45	TAN20_T55

Chapter 4

Materials and methods

Laboratory scale experiments with test conditions as summarized in Table 1 have been carried out to determine the quantity (total absolute flux) and quality (m% NH_3) of the produced MD permeate gas and to determine whether MD could be a suitable gas production technology for the From pollutant to power project. This chapter describes the methods and materials used to carry out the experiments (paragraphs 4.1 to 4.4) and to process experimental data (paragraphs X and Y). Tests have been executed in the Sanitary Engineering water laboratory at the Faculty of Civil Engineering and Geosciences of Delft University of Technology.

4.1 Feed solution preparation

Synthetic NH_4HCO_3 solutions were used to simulate reject water and urine in the laboratory scale experiments (paragraph 2.1.2). In preparation of the experiments, a weighed mass of demineralized water (demiwater) was first heated until the intended temperature was reached. To obtain the desired TAN concentrations of 1.5, 12 and 20 g/L, respectively 6.6, 52.6 and 87.7 g/L of NH_4HCO_3 should be dissolved based on calculations with molar masses of 18.0 g/mol for NH_4^+ and 79.1 g/mol for NH_4HCO_3. Sigma-Aldrich NH_4HCO_3 (purity $\geq$ 99.5%) was dissolved in the preheated demiwater in amounts that were generally 1.3 times higher in order to obtain higher initial concentrations (Appendix X), as TAN concentrations were expected to decrease over the experimental run time. Subsequently, a noted volume of Boom 32% technical grade NaOH solution from Boom Laboratoriumleverancier was added to increase the pH value of the solution up to approximately 10. After the additions of NH_4HCO_3 and NaOH solution, the feed solution mixture was left in a closed bottle under continuous stirring until a stable pH value was reached.

4.2 Measurements and equipment

The following parameters were measured in the laboratory experiments, using the equipment as described below:

- *Electrical conductivity (EC), pH and temperature:*
  EC, pH and temperature were measured simultaneously using a WTW digital precision meter Multi 3630 IDS in combination with a calibrated WTW TetraCON 925 EC sensor and a calibrated WTW IDS SenTix 940 pH sensor. Measurement data was automatically registered every 30 seconds in a Microsoft Excel document on an attached laptop.

- *Mass of bottle with feed solution:*
  The mass of the bottle filled with feed solution was measured using a Kern PCB 6000-1 digital precision balance. Measurement data was automatically registered every 30 seconds in a Windows Notepad document on an attached laptop using KERN Software Balance Connection for data transmission.

- *Feed solution TAN concentration:*
  Feed solution TAN concentration was measured every 15 to 20 minutes over the experimental run time using MACHEREY-NAGEL NANOCOLOR Ammonium 200 and Ammonium 2000 tube tests. In the test tubes, all TAN is converted into NH_3. Samples were introduced into the test tubes using a Thermo Scientific 100–1000 μL Finnpipette F1 pipette and analysed using a spectrophotometer NANOCOLOR VIS II.

4.3 Experimental set-up

The experimental set-up that was used is shown in Figure 4.1 and 4.2. A closed DURAN laboratory glass bottle of volume 0.5 or 1.0 L containing the feed solution prepared as described in paragraph 4.1 was placed on an IKA RH Digital KT/C magnetic stirrer hot plate combination. The total was placed on the digital precision balance described in paragraph 4.2, that was attached to a laptop for data logging. An IKA Ikatron ETC 1 temperature controller was connected to the magnetic stirrer hot plate combination and placed in the feed solution bottle to keep the solution at a set temperature. Sensors for EC, pH and temperature measurement (described in paragraph 4.2) were placed in the feed solution and connected to the laptop for data logging as well. Feed solution was pumped from the feed solution bottle to a membrane module using a Watson-Marlow Sci-Q 300 Series peristaltic pump. The membrane module used in the experimental set-up was a Sterlitech CF042 acrylic crossflow cell with a 42 cm^2 active membrane area (Figure 4.3). Sterlitech flat-sheet PTFE membranes with PP backing and 0.1 μm pore size were placed in the membrane module, as well as Sterlitech CF042 PP feed and permeate spacers. A diamond-shaped 47 mil spacer was placed in the feed side cavity of the membrane module to increase feed flow turbulence and a diamond-shaped 31 mil spacer was placed in the permeate side cavity of the membrane module. A KNF N816.3KT.45.18 vacuum pump was used to keep a partial vacuum in and remove permeate gas from the permeate side cavity of the membrane module. Permeated NH_3 and H_2O gases were trapped in an acidic solution prepared with demiwater and Sigma-Aldrich 0.1–5 M H_2SO_4 (purity $\geq$ 99.999%) solution. The acid trap bottles were placed in ice baths for cooling to prevent gases from evaporating and subsequently condensing in the vacuum pump or escaping into the air.

4.4 Experimental procedure and conditions

After feed solution preparation and pH stabilization (paragraph 4.1), data logging was started. Subsequently, flow was started by switching on the feed pump. Feed flow rates were calculated based on a selected Re value of 500 (resulting in unsteady flow according to studies on spacer-filled flow channels; paragraph 2.3.3). Corresponding cross flow velocities were 10–17 cm/s, depending on feed solution temperature (Appendix B). The feed pump was calibrated in order to translate crossflow velocities to pump speed settings. As soon as the membrane module was filled with feed solution, a partial vacuum of 1500 Pa was created by switching on the vacuum pump. A VMD configuration was chosen to create a gas consisting of NH_3 and H_2O without influences of other components on the permeate side of the membrane. 1500 Pa was the lowest pressure that could be created with the used vacuum pump and was selected to maximize driving forces. The system was left to stabilize for 10 to 30 minutes after switching on the vacuum pump.

Feed solution samples were taken every 15 to 20 minutes over an experimental run time of 1.5 to 2 hours. Run time was started at the first sampling moment. Samples were taken using a 1 mL BD Plastipak syringe, injecting the needle in the tube between feed pump and membrane module. Samples were diluted in an acidic solution prepared with demiwater and Sigma-Aldrich 0.1–5 M H_2SO_4 (purity $\geq$ 99.999%) solution to impose instantaneous conversion of NH_3 gas into NH_4^+ to prevent the gas from escaping into the air. The acidic solution mass was weighed before and after addition of the feed solution sample to enable calculation of the dilution factor.

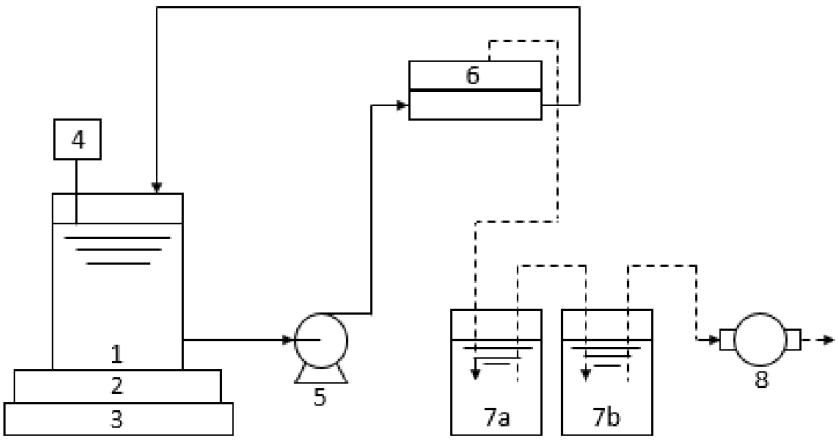

1. Feed solution
2. Magnetic stirrer hot plate combination
3. Digital balance
4. Sensors (EC, pH, T)
5. Feed pump
6. Membrane module
7. Cooled acid traps (a,b)
8. Vacuum pump

Liquid
Gas

Figure 4.1: Experimental set-up (schematically).

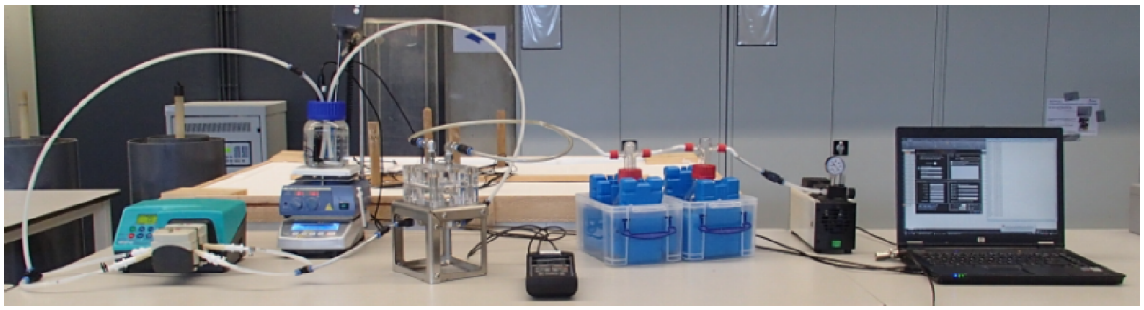

Figure 4.2: Experimental set-up.

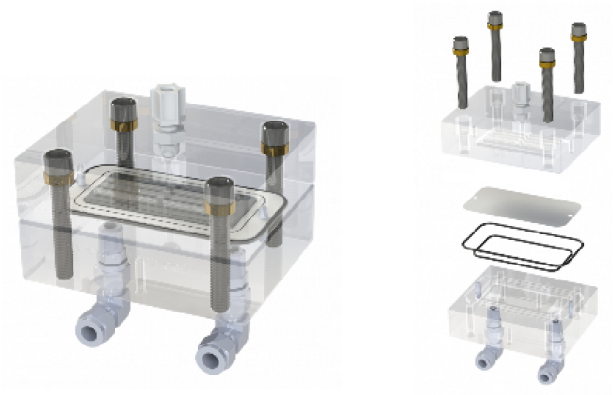

Figure 4.3: Sterlitech membrane module [55].

At the end of each run, the system was flushed with demiwater for several minutes. Afterwards, pumps were switched off and the membrane module was opened to dry the cell, membrane and spacers. Tubes were dried as well, using compressed air. All experiments were executed in duplo and control tests with demiwater (0 g TAN/L) were carried out as well.

4.5 Data processing

Data obtained from mass logging and TAN concentration measurements were used to determine the total, NH_3 and H_2O fluxes (J_{tot}, J_{NH_3} and J_{H_2O}, respectively) through the MD membrane. Data obtained from EC, pH and temperature measurements mainly functioned as a control of test conditions and to check whether processes occurred as expected (explained further in paragraph 5.2.1). Data on pH were also used in PHREEQC simulations for the determination of K_g (paragraph 4.5.4). Time step durations in data processing calculations were based on the interval between two subsequent TAN concentration measurements. In the rest of this report, TAN concentration is abbreviated to C_{TAN}.

4.5.1 Total ammonia nitrogen concentration over experimental run time

Data processing of C_{TAN} measurements included three steps:

1. Calculation of $C_{TAN,NH_3,feed}$ from $C_{TAN,NH_3,measured}$. Samples were diluted in an acidic solution (paragraph X) and this is corrected for by a dilution factor. The changing density of the feed solution was taken into account in calculation of the dilution factor.

2. Calculation of $C_{TAN,feed}$ from $C_{TAN,NH_3,feed}$. TAN was measured as NH_3 in the test kits used for analysis (paragraph X). $C_{TAN,NH_3,feed}$ was converted to $C_{TAN,feed}$ using a TAN average molar weight derived from PHREEQC simulations results for the considered pH, temperature and C_{TAN}.

3. Fitting of an exponential trendline through $C_{TAN,feed}$ data points over experimental run time. An exponential trendline is characteristic for first order kinetics.

4.5.2 Transmembrane fluxes over experimental run time

Data processing to determine the transmembrane fluxes J_{tot}, J_{NH_3} and J_{H_2O} included five steps:

1. Determination of J_{tot} per time step:

$$J_{tot} = \frac{\Delta m_{tot}}{A \Delta t} \tag{4.1}$$

   In this equation, Δm_{tot} is the difference in mass measured over the duration of the time step Δt. As mentioned in the introduction of this section, a time step was defined as the interval between two subsequent C_{TAN} measurements. A is the active membrane surface area.

2. Fitting of a linear trendline through J_{tot} data points over experimental run time. The calculated value of J_{tot} was plotted for each time step at time t in the middle of the time step. A linear trendline was fitted through the data points obtained after system stabilization (further explained in paragraph 5.2.2).

3. Determination of J_{NH_3} per time step:

$$J_{NH_3} = \frac{\Delta m_{NH_3}}{A \Delta t} \tag{4.2}$$

   Feed solution masses required to calculate the removed NH_3 mass Δm_{NH_3} over a time step Δt were calculated by multiplication of the feed volume with C_{TAN} for the beginning and for the end of Δt. Feed volumes were not measured, but calculated by division of the feed mass

over the feed density. Feed mass at a time t was taken as the initial feed mass minus the total flux up to time t and sampling volumes. Feed density was iteratively determined using calculated fluxes. Initital feed density was calculated based on the amounts of demiwater, NH_4HCO_3 and NaOH in the feed solution.

4. Fitting of an exponential trendline through J_{NH_3} data points over experimental run time. The calculated value of J_{NH_3} was plotted for each time step at time t in the middle of the time step.

5. Calculation of J_{H_2O} by subtraction of the trendline value for J_{NH_3} from the trendline value for J_{tot}:

$$J_{H_2O} = J_{tot,trendline} - J_{NH_3,trendline} \tag{4.3}$$

4.5.3 Permeate quantity and quality from duplo test results

Results from duplo tests for each test combination in Table 1 were averaged via their trendlines in three steps:

1. Determination of the time of occurence of the selected C_{TAN}. Measurements were conducted around the intended concentrations of 1.5, 12 and 20 g/L. The moment in time t at which the intended C_{TAN} was attained was recalculated from the J_{NH_3} trendline equation.

2. Determination of J_{tot}, J_{NH_3} and J_{H_2O} at time t determined in step 1 using the trendline equations of J_{tot} and J_{NH_3} and Equation 4.3.

3. Determination of the average permeate quantity and quality (defined in paragraph 13.1) from duplo runs for the same test conditions, with the fluxes for the intended values of C_{TAN} obtained in step 2. As fluxes are expressed as masses per unit of membrane area and time, the definition of permeate quality given in Equation 1.1 might also be written as:

$$m\%\, NH_3 = \frac{J_{NH_3}}{J_{tot}} \cdot 100\% \tag{4.4}$$

4.5.4 Global mass transfer coefficient from duplo test results

Values of K_g were calculated for NH_3 and H_2O (including demiwater) over individual experimental runs first and subsequently averaged for duplo tests of each test combination (Table 1), in five steps:

1. Simulations in PHREEQC with concentrations according to the C_{TAN} trendline and pH values according to a trendline fitted through pH measurement results, to obtain the vapor pressures $p_{NH_3,feed}$ and $p_{H_2O,feed}$ at times t at the beginning and end of each time step over an experimental run.

2. Calculation of $p_{NH_3,permeate}$ and $p_{H_2O,permeate}$ with permeate NH_3 and H_2O molar fractions based on partial fluxes and the partial vacuum pressure of 1500 Pa:

$$p_{i,permeate} = \frac{mol_{i,permeate}}{mol_{tot,permeate}} \cdot 100\% \tag{4.5}$$

   In this equation, i is NH_3 in the calculation of $p_{NH_3,permeate}$ and H_2O in the calculation of $p_{H_2O,permeate}$. Permeate vapor pressures were determined for times t at the beginning and end of each time step over an experimental run.

3. Calculation of K_g based on fluxes and vapor pressure differences at times t at the beginning and end of each time step over an experimental run based on Equation 2.34:

$$K_{g,i} = \frac{J_i}{p_{i,feed} - p_{i,permeate}} \tag{4.6}$$

   In this equation, i is NH_3 in the calculation of K_{g,NH_3} and H_2O in the calculation of K_{g,H_2O}.

4. Determination of the average K_g over an experimental run. This is done by averaging the values of K_g calculated for the times t at the beginning and end of each time step within the experimental run.

5. Determination of the average K_g from duplo tests for each test combination in Tabel 1.

Chapter 5

Results and discussion

5.1 Demiwater permeation tests

The fluxes obtained in demiwater permeation tests are presented in Figure 5.1 as averaged results from duplo tests per temperature setting. A decrease in flux was observed at the beginning of the runs at 25 and 35 °C, which is attributed to a low initial resistance in membrane pores. Pores do not go straight through an MD membrane, but have curves and edges (Figure 2.6). At the beginning of a run, when pores are still (relatively) empty, the resistance is low. As the pores get filled with transported molecules, resistance increases [56]. This phenomenon is more explicit at lower temperatures than at higher temperatures because of the lower fluxes at lower temperatures. The lower the flux, the longer it takes for the pores to fill and for the system to stabilize. At higher temperatures of 45 and 55 °C, a more or less constant flux is shown directly from the start of the runs. Demiwater runs were all started at the same point of time after starting the feed and vacuum pumps.

The global mass transfer coefficient K_g for demiwater for the used membrane system and settings was calculated as explained in paragraph 4.5.4 and is included in Figure 20 (paragraph 5.3).

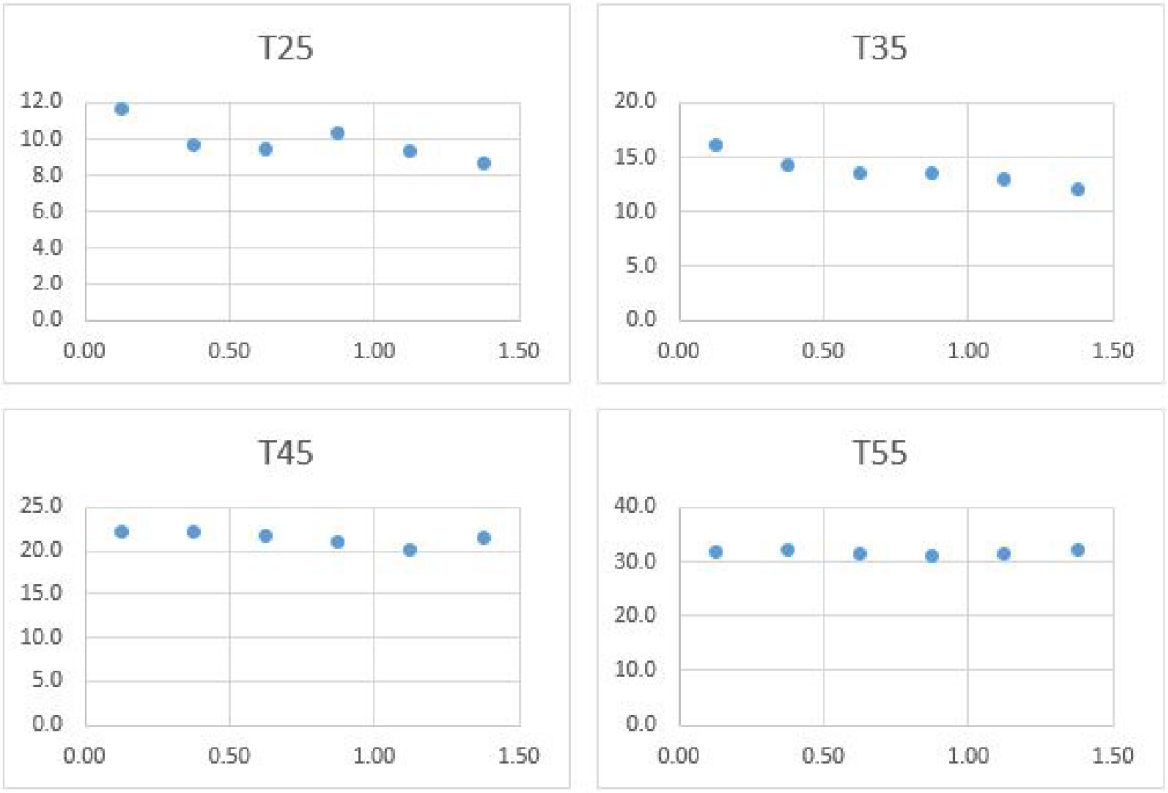

Figure 5.1: Demiwater permeation tests for selected temperatures with flux ($kg/m^2/h$) on all y-axes and run time (h) on all x-axes.

5.2 Experimental data

5.2.1 Obtained data per experimental run

An example of measurement data obtained per experimental run is shown in Figure 5.2 (for experimental test conditions of TAN1.5 and T25). As mentioned in paragraph 4.5, data on EC, pH and temperature were mainly meant for checking whether processes were happening as expected

and data on feed mass and C_{TAN} were meant for further data processing and calculations.

Temperature was practically constant over all experimental runs. Only small deviations of 1–2% from set temperatures were observed, which were due to the temperature controller switching the heating mechanism of the magnetic stirrer hot plate combination on and off to keep temperature at the set value. EC showed an increase of 2–30% over experimental run times depending on temperature, C_{TAN}, initial solution volume and total run time (Appendix F). The increase in EC is explained by the evaporation of liquid solvent, concentrating ions in a smaller solution volume. pH decreased over time, due to the consumption of base (OH^-) by NH_4^+ in the reaction described by Equation 2.12 in order to counteract the shift in equilibrium caused by the removal of NH_3 at the membrane surface (Le Chateliers principle [37]).

The mass of the feed solution decreased over time, as expected, because of gas transfer through the MD membrane from feed to permeate side. At sampling moments, a (small) sudden drop in mass is observed. C_{TAN} in the feed solution also decreased over time, as NH_3 gas is removed from the feed solution at the membrane surface and is more volatile than H_2O [17]. The removal shows an exponential trend, characteristic of first order kinetics.

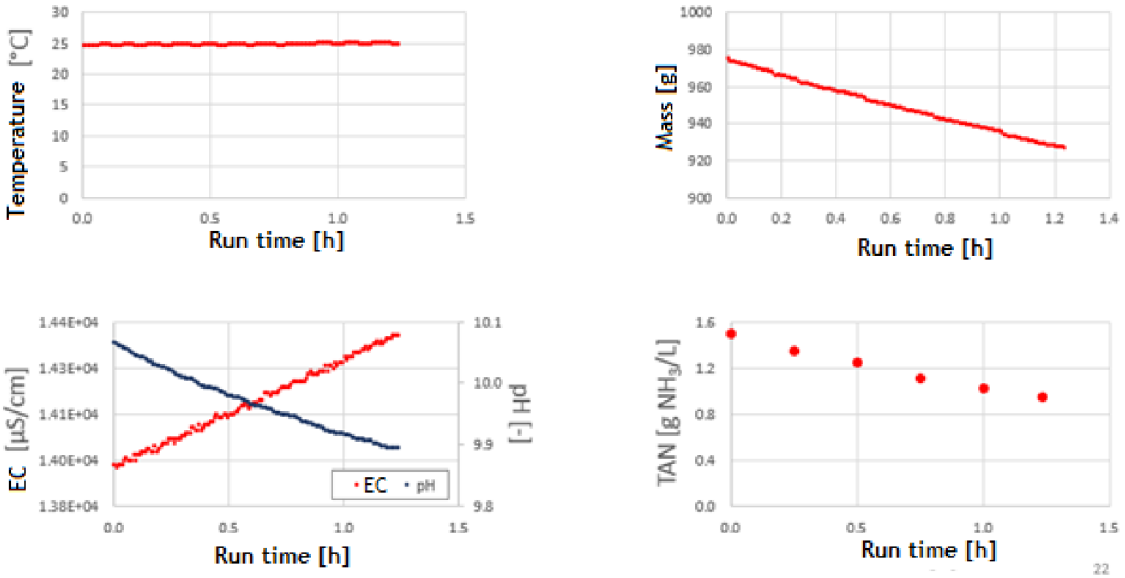

Figure 5.2: Obtained data per experimental run (example TAN1.5 and T25).

5.2.2 Calculated transmembrane fluxes per experimental run

It was observed that total transmembrane fluxes decreased over time during experimental runs. Generally speaking, there were two parts of flux decrease. The first part, that mainly occurred at the beginning of experimental runs at feed temperatures of 25 °C and sometimes of 25 °C, is attributed to system stabilization (as explained in paragraph 5.1). For the calculation of total flux trendlines, data points that belonged to this first part of flux decrease were left out. At feed temperatures of 45 and 55 °C, system stabilization seemed to have occurred before the start of the experimental runs. For those runs, all data points were taken into account for total flux trendline calculations.

The second part of flux decrease, observed after system stabilization, is attributed to an increase in ionic strength. As explained in paragraph 5.2.1, the increase of EC over experimental run time is explained by the evaporation of liquid solvent, concentrating ions in a smaller solution volume. An

increase in ionic strength results in a lower H_2O activity and a lower H_2O mole fraction. According to Raoult's law (Equation 2.29), this leads to a decrease in H_2O vapor pressure (paragraph 2.2.1). Figure 5.3 shows the absolute values of the variations of J_{tot} and EC over time (absolute values of the slopes of the graphs of J_{tot} and EC over experimental run time; averaged for duplo tests of the same test conditions) in order to compare flux decrease and EC increase. Indeed, it is seen that in general EC increase coincides with flux decrease. Figure 5.3 also shows that EC increase and flux decrease are higher at higher temperatures for a fixed C_{TAN}. Higher EC increase at higher temperatures is attributed to the faster H_2O evaporation (higher J_{H2O}) at higher temperatures. The higher ionic strength results in larger decreases in H_2O activity and mole fraction, resulting in a higher decrease in J_{H2O}. Polarization effects might intensify the decrease in J_{H2O}, when the increase of ionic strength is even stronger at the membrane surface, where evaporation takes place. In Figure X it can be seen that in the demiwater permeation tests, in which no other ions than H^+ and OH^- from the water ionization equilibrium are present in the feed solution, a constant flux was obtained after system stabilization. This reinforces the hypothesis that the second part of flux decrease is related to the increased ionic strength of the feed solution over experimental run times. Also in literature, flux decrease over experimental run time was observed [56].

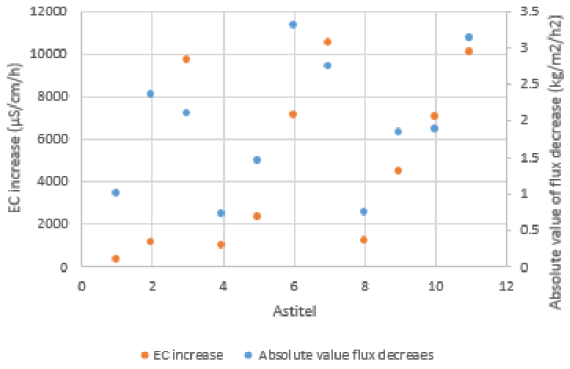

No.	Temperature	Absolute value flux decrease	EC increase
1	25	0.99	349
2	35	2.35	1158
3	55	2.09	9654
4	25	0.71	1013
5	35	1.44	2324
6	45	3.30	7091
7	55	2.74	10503
8	25	0.75	1200
9	35	1.83	4433
10	45	1.88	7032
11	55	3.14	10033

Figure 5.3: Absolute value of total flux decrease and EC increase.

For some experimental runs, the opposite effect of a lower flux at the beginning of the experimental run was observed. This might be related to the point in time at which the experimental run was started. The time between the moment of switching on feed and vacuum pumps and the start of measurements might have been to short for the partial vacuum to fully establish in the membrane module. Experimental runs were not all started at the same moment after the start of the system.

5.3 Global mass transfer coefficient

As described in paragraph 2.3, the mass transfer coefficients K_{OV} and K_g can be divided into three separate mass transfer coefficients corresponding to the feed, membrane and permeate mass transfer systems. K_m could not be determined experimentally in this master thesis study and not enough data on membrane characteristics was made available by the membrane manufacturer to calculate K_m. Therefore, only the global mass transfer coefficient K_g including all resistance effects was calculated from obtained experimental data.

Figure 5.4 shows the global mass transfer coefficient K_g for H_2O, NH_3 and pure water (0 g TAN/L). It can be observed that K_g is dependent on both temperature and C_{TAN}. Overall, K_g decreases with increasing C_{TAN} (and corresponding higher NaOH additions to increase pH in the buffer system) and with increasing temperature. This is attributed to increased polarization effects and resulting higher resistances to mass transfer at higher concentrations and temperatures (paragraph 2.3.3).

Figure 30 also shows that K_{g,H_2O} was higher than K_{g,NH_3} in all experiments, which is attributed to the fact that the concentration H_2O in the feed solution is much higher than the concentration NH_3 in all solutions. Polarization effects have a different character for H_2O and NH_3, as discussed in paragraph 2.3.3. Polarization effects for H_2O lower the H_2O vapor pressure at the membrane surface, but H_2O molecules are still present and available for evaporation. Polarization effects for NH_3 on the other hand cause a depletion of NH_3 molecules at the membrane surface, thereby preventing evaporation from taking place.

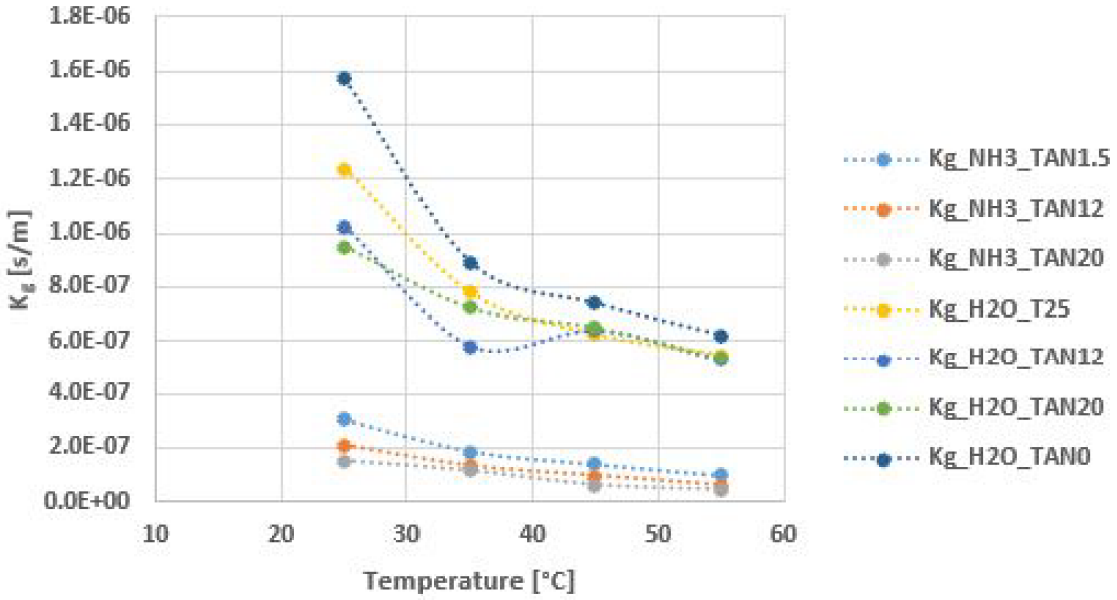

Figure 5.4: Global mass transfer coefficients K_g over temperature and TAN concentration.

5.4 Permeate quantity

As one of the goals of this thesis research was to determine the influence of temperature and C_{TAN} on permeate quantity, J_{tot} is presented both as function of temperature (Figure 5.5) and as function of C_{TAN} (Figure 5.6). As can be seen in the graphs, J_{tot} increases with temperature (from 25 to 55 °C increase is from 7.5 to 27.3 kg/m^2/h) and is more or less equal for all three selected TAN concentrations. This is due to the major contribution of J_{H_2O} to J_{tot} and the fact that H_2O vapor pressures are only slightly dependent on C_{TAN} for the selected range of C_{TAN} (paragraph 3.2.2). The increase in absolute flux is not as clearly exponential as might be expected from H_2O vapor pressure calculations based on the Antoine equation and Raoult's law (paragraph 2.2.1). This is attributed to the increased effect of (mainly) temperature polarization effects at higher temperatures, resulting in lower values of K_{g,H_2O} and thereby to lower J_{H_2O} (polarization effects are not included in PHREEQC equilibrium simulations). Total fluxes obtained in experiments with NH_4HCO_3 solutions (Figure 5.5) generally showed to be lower than total fluxes obtained in demiwater permeation tests (Figure 5.1). This is attributed to an increased ionic strength (as explained in paragraph 2.1.2).

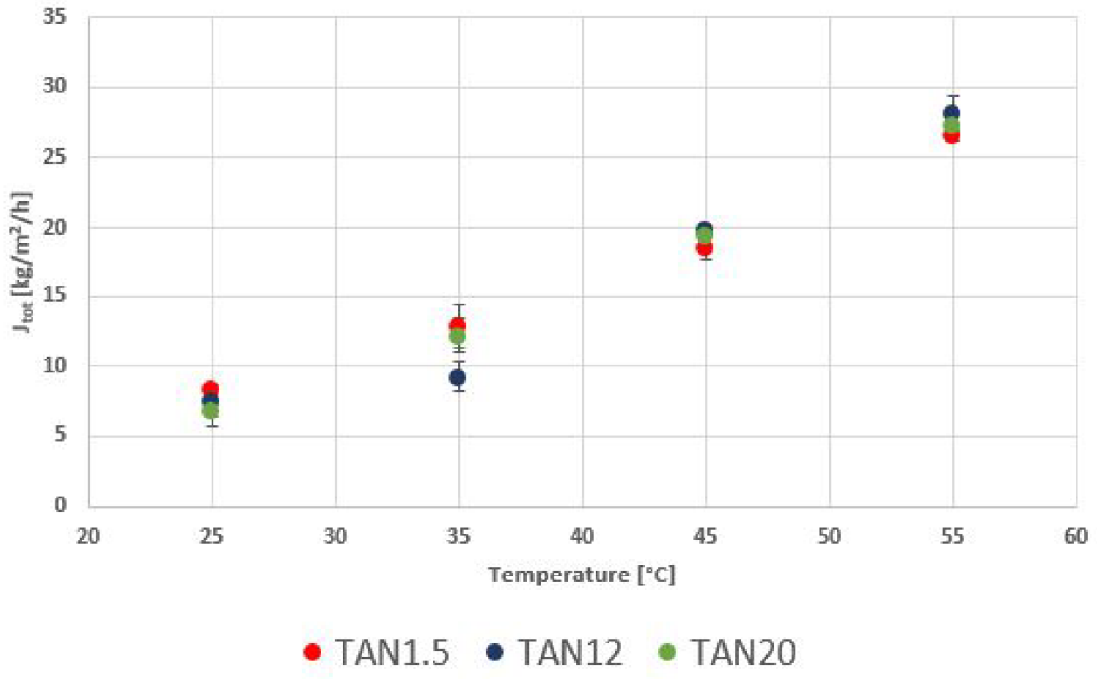

Figure 5.5: Absolute total flux as function of temperature

5.5 Permeate quality

Also permeate quality (as defined in paragraph 1.3.1) is presented both as function of temperature (Figure 5.7) and as function of C_{TAN} (Figure 5.8). From these figures, it can be seen that a higher permeate quality was obtained at lower temperatures. This matches the expectations based on theory (Chapter 2) and PHREEQC simulations (Chapter 3). The relatively low obtained permeate quality at 25 °C is attributed to the TAN equilibrium that has not shifted completely to the side of NH_3 yet (especially at lower temperatures and higher TAN concentration; paragraph 3.2.1). Would pH values of 11 or higher be applied, resulting in a NH_3/TAN ratio of approximately 1 for all selected values of C_{TAN} and all selected temperatures, higher fluxes would be expected at

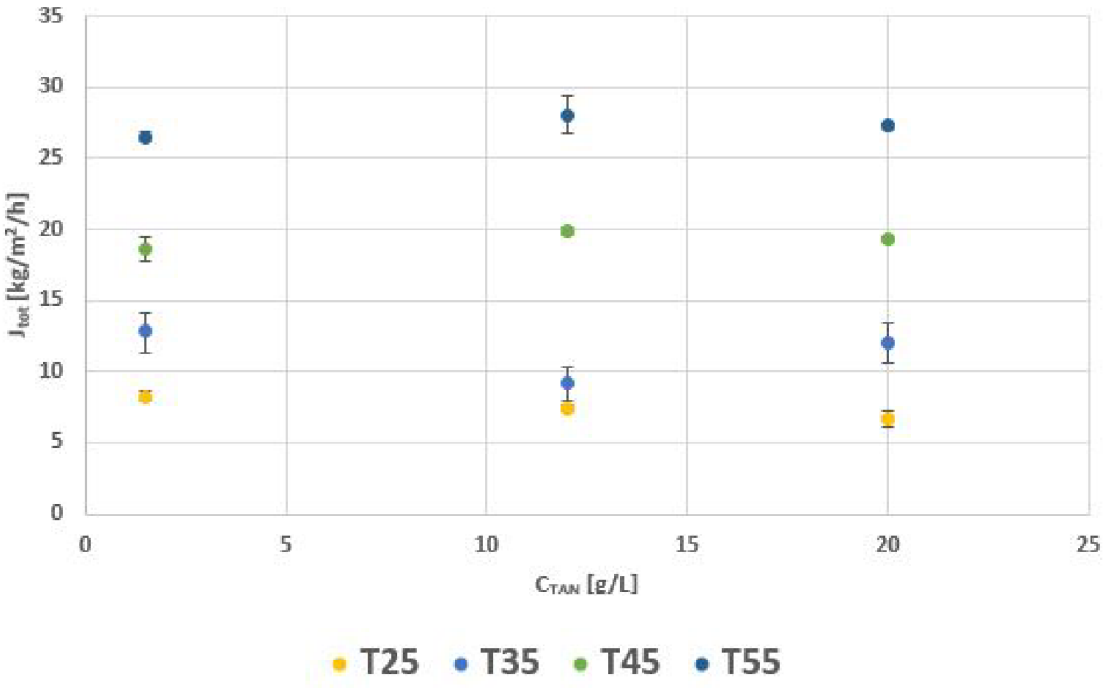

Figure 5.6: Absolute total flux as function of C_{TAN}

25 °C. The decrease in permeate quality with temperature is attributed to the strong increase of H_2O vapor pressure at temperatures above 30 °C compared to the increase of NH_3 vapor pressure (Appendix D).

As mentioned in paragraph 1.3 and presented in Appendix A2, the minimum MD permeate quality is some value between 5 and 10 m% NH_3. The 10 m% NH_3 at which the SOFC has proved to work within the *From pollutant to power* project is shown to be obtained at temperatures of 25 and 35 °C for a feed solution of 20 g TAN/L. For TAN concentrations of 12 and 20 g/L at temperatures of 25, 35 and 45 °C, m% NH_3 showed to be higher than 5. Thus, these combinations of conditions might result in a SOFC fuel with sufficient quality as well. Further research on required SOFC fuel gas characteristics and SOFC performance under produced NH_3 fuel gases will be carried out within the *From pollutant to power* project. The anomaly in m% NH_3 for the 12 g TAN/L solution at a temperature of 35 °C is attributed to measurement errors.

Trendlines through datapoints in Figure 5.8 show a good fit ($R^2 > 0.97$ for all trendlines). Trendline equations were used for forecasting of permeate quality at higher TAN concentrations than 20 g/L. Figure 5.9 shows that, based on this estimation, it is practically impossible to obtain a 10 m% NH_3 permeate gas at temperatures of 45 and 55 °C, as to do so C_{TAN} must be higher than 100 g/L. Concentration factors (as defined in paragraph 3.1) were determined as well and are shown in Figure 5.10. It is shown that concentration factors decrease not only with temperature, but also with TAN concentration. Linear trendlines through datapoints in Figure 5.10] show a good fit as well ($R^2 > 0.98$ for all trendlines) and could be used to estimate the concentration factors (and thus, permeate quality) that could be obtained for combinations of C_{TAN} and temperature. Concentration factors were in the same range as concentration factors obtained in studies found in literature (paragraph 3.1).

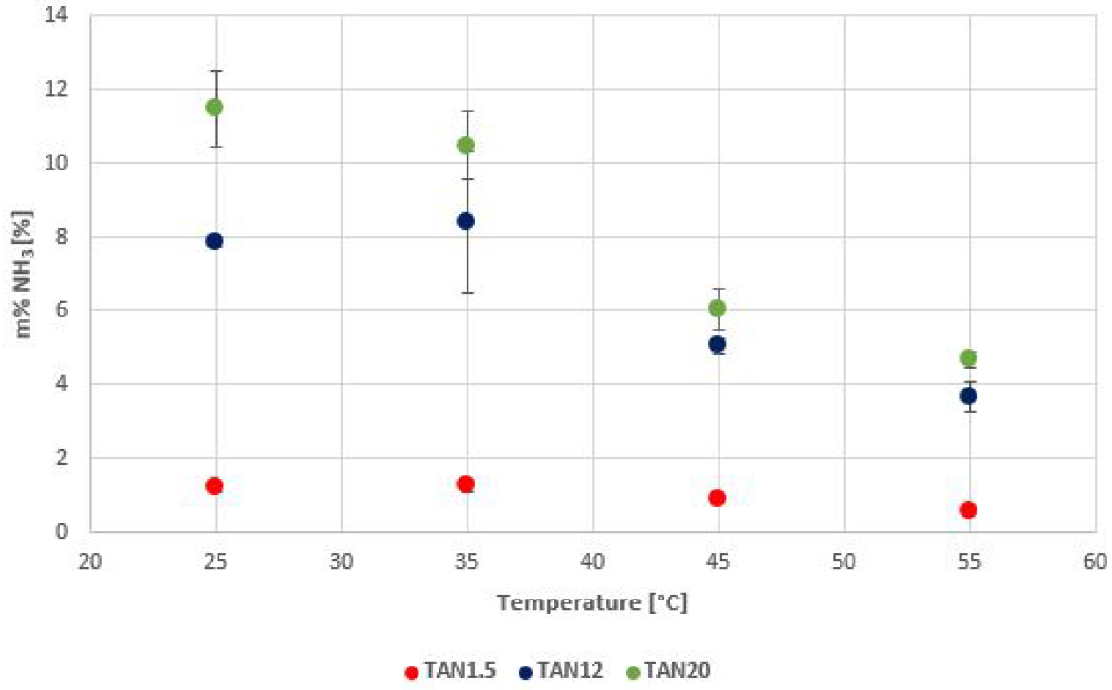

Figure 5.7: Permeate quality as function of temperature

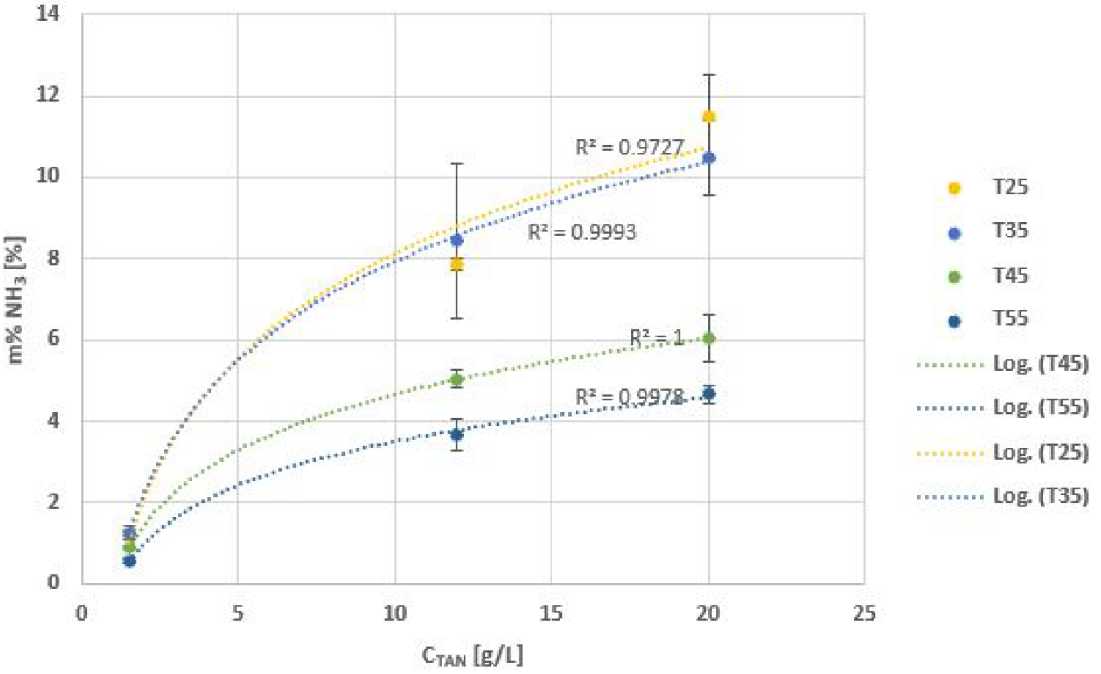

Figure 5.8: Permeate quality as function of C_{TAN}

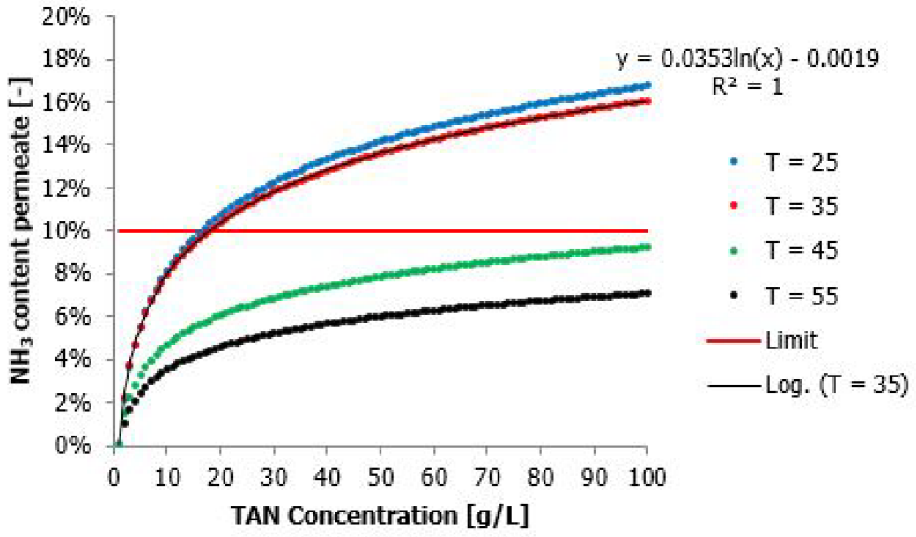

Figure 5.9: Permeate quality forecasting

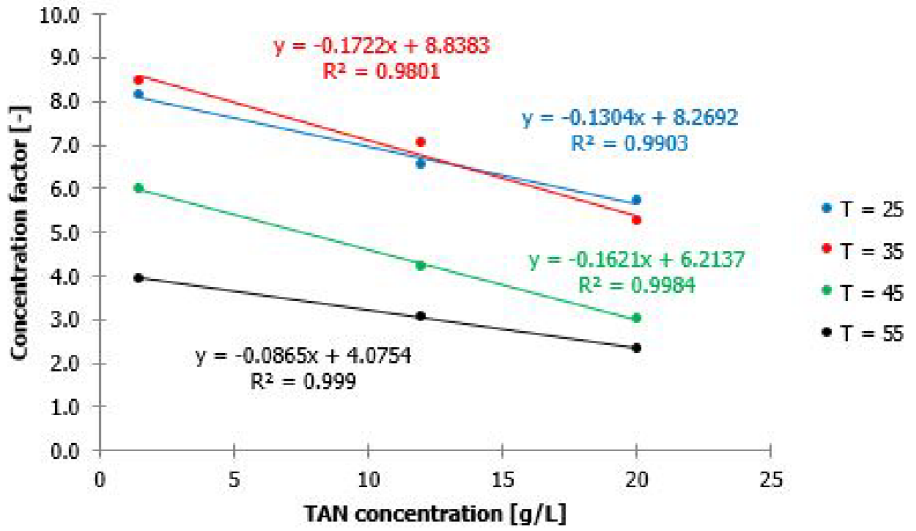

Figure 5.10: Concentration factors

5.6 Nitrogen removal as ammonia gas flux

N removal is presented as J_{NH_3} in Figure 5.11. As can be seen, J_{NH_3} depends on both temperature and TAN concentration, as expected due to the dependency of the NH_3 driving force on these parameters (paragraph 2.2.1). Higher concentrations and higher temperatures generally lead to higher fluxes; however, this is not in a clear exponential relationship as might have been expected based on vapor pressure calculations through Henry's law. This is attributed to the increased effect of polarizations at higher temperatures, resulting in lower values of K_{g,NH_3} and thereby to lower J_{NH_3}. As explained in paragraph 5.3, the polarization effects for NH_3 result in a depletion of NH_3 molecules at the membrane surface, thereby preventing evaporation from taking place.

Theoretically, N removal obtained by MD in this master thesis study could be compared to N removal in conventional and Anammox N removal processes. However, in the *From pollutant to power* project the focus of the gas production step is on the performance of technologies in terms

of gas production and not in terms of N removal. The experimental results obtained in this study show that the MD technology performance worsens with a decrease in TAN concentration. N removal up to standard effluent requirements (paragraph 1.1.1) would lead to concentrations and subsequently also vapor pressures so low that NH_3 transmembrane fluxes would probably not occur at all; MD should be considered as an NH_3 gas production technology and not as an TAN removal technology. A gas production step using MD technology would be expected to deliver a residual stream, instead of an effluent that can be discharged on surface waters directly. An effluent that does meet standard effluent requirements might be produced in another step within the *From pollutant to power* project, for example in a concentration step.

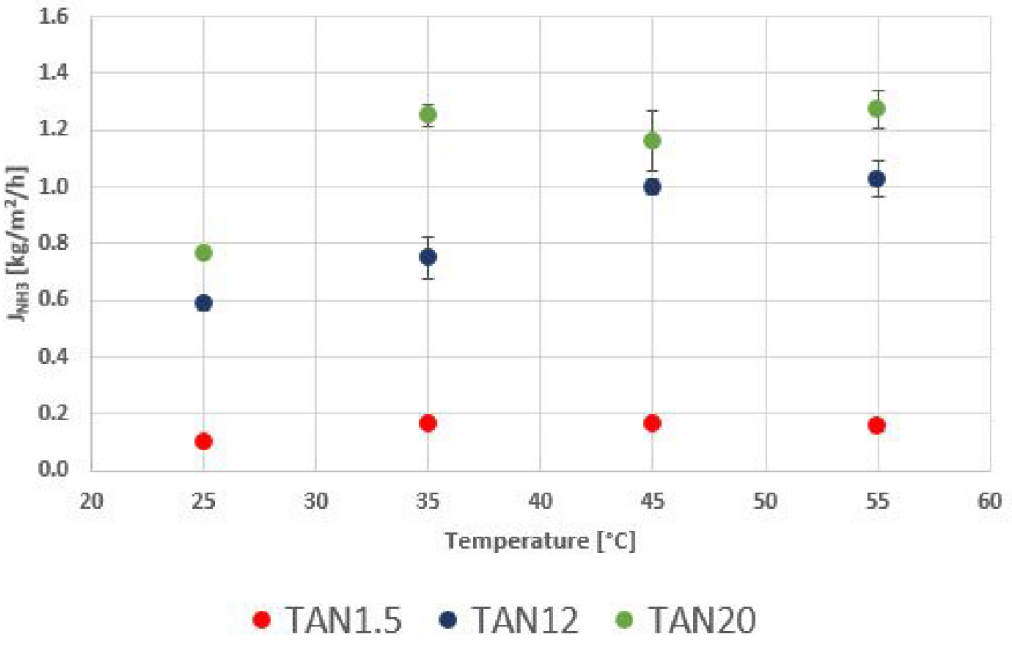

Figure 5.11: N removal expressed as NH_3 flux

5.7 Suitability of membrane distillation in *From pollutant to power*

5.7.1 Permeate quantity versus permeate quality

Obtained experimental results show that MD could be a suitable option for the production of an SOFC fuel gas on the conditions of a preceding concentration step, operation in a low temperature range (25 to 35 °C) and under basic conditions (pH > 10). Under these conditions, a permeate quality could be obtained such that it can be fed to an SOFC directly. It should be noted, however, that due to the low operation temperatures required to obtain a high permeate quality, permeate fluxes were relatively low. The importance of a concentration step before MD gas production is demonstrated, as with 1.5 g TAN/L feed solutions (simulating reject water) permeate quality was never high enough for an SOFC to function. In Figure 5.9, it can be seen that even a permeate quality of 5 m% NH_3 would be hard to obtain with a 6 g TAN/L solution (simulating urine) as well. An optimum should be found between permeate quantity and quality in combination with SOFC performance.

5.7.2 Energy considerations

To decide on whether MD could be a suitable technique in the *From pollutant to power* project, it must be considered in combination with concentration step and SOFC research. An overall mass and energy balance could show whether the SOFC electrical and thermal energy suffice to perform concentration and gas extraction steps with the produced gas, that is, whether an overall energy neutral or producing system could be created. Thus, an overall mass and energy balance for the *From pollutant to power* project would be needed to decide on whether MD is a suitable technology for gas production within the project. It should be mentioned that since the thermal energy requirement for heating of a feed solution to MD temperatures is usually the main energy demand in VMD (paragraph 3.3; with VMD usually applied at higher temperatures than the temperatures considered in this study), it could be beneficial to perform VMD at the lower temperatures that result in sufficient SOFC fuel gas quality as found in this study.

Three possible sources of thermal energy that could possibly be used to raise MD feed solution temperatures are:

- *SOFC thermal energy:*
  SOFC thermal energy is contained in off-gases. Heat exchangers would be needed to use the thermal energy for heating of the feed solution. This will result in thermal energy losses dependent on the efficiency of the heat exchangers. This is not further elaborated upon in this study.

- *Heat contained in anaerobic digestion effluent:*
  The anaerobic digestion process is carried out at temperatures of 30 to 38 °C [67]. When this heat could be contained in the effluent stream, less or no thermal energy would be needed to heat the feed stream for the MD gas production step. It should be mentioned, however, that higher temperatures are not necessarily beneficial for concentration technologies. At the moment, ED is seen as a promising concentration technology within the *From pollutant to power* project. Literature shows that temperatures above room temperature are not favorable for the ED process [60]. When ED would be applied as concentration technology, reject water would therefore probably be brought to room temperature and thus, heat contained in anaerobic digestion effluent would not be available as a source of thermal energy. In combination with other concentration technologies, it might be possible to us this source of thermal energy.

- *MD residual heat:*
  When multiple MD stages are applied, the heat contained in the feed solution that has passed the MD membrane of the final step could be used to heat new incoming feed water. Also in this case, heat exchangers would be needed to transfer thermal energy from one stream to the other.

5.8 Discussion on materials and methods

Some remarks should be made in relation to the materials and methods applied in this thesis study. First of all, no mass balancing was done regarding total and N masses during the laboratory experiments. Only mass removal from the feed solution was measured, under the assumption that all removed mass was evaporated through the MD membrane. As all experiments have been carried out with a closed system, it is expected that his is a valid assumption.

Secondly, it was assumed that CO_2 vapor pressures could be neglected due to the pH value of 10 applied in the experiments. This assumption was based on PHREEQC simulation results but has not been verified through experiments. When a CO_2 flux would take place as well, this would only influence the calculated H_2O fluxes. NH_3 flux was calculated based on direct measurements of its concentration and m% NH_3 was determined based on NH_3 flux and total fluxes. Thus, the results

related to these calculations would not be influenced directly.

Trendlines have been used in the determination of concentrations and fluxes (paragraph 4.5). As not all data points could always be included due to system stabilization times (paragraph 5.2), effective experimental run times were sometimes short. Also, during experimental runs conditions such as pH and ionic strength decreased or increased. Flux and concentration calculation results might therefore deviate from results that would have been found when these values would have been kept constant. However, as average values of duplo tests have been used for analysis, it is expected that extreme deviations are balanced out.

Chapter 6

Conclusions

Through literature research, PHREEQC simulations and experiments, the following answers to the research questions as stated in paragraph 1.3.2 have been found:

1. How do temperature and ammonia nitrogen concentration influence permeate quantity and quality in vacuum membrane distillation (at selected test conditions)?

   Generally, increase of temperature leads to higher fluxes due to higher vapor pressures. Therefore, it can be said that temperature has a positive influence on permeate quantity. As not only NH_3 evaporates through the membrane but also H_2O, temperature has a negative influence on permeate quality. Vapor pressure of H_2O shows a stronger increase with temperature than NH_3 vapor pressure, especially at higher temperatures.

   Ammonia nitrogen concentration does influence permeate quality positively, as the vapor pressure of NH_3 is increased. It should be noted, however, that conditions favoring the formation of NH_3 in the TAN equilibrium should be applied, as TAN can only be removed in the form of NH_3. TAN concentration does not significantly influence permeate quantity as H_2O flux is predominant over NH_3 flux.

2. Could membrane distillation be a suitable technology for the production of an ammonia fuel gas for solid oxide fuel cells within the *From pollutant to power* project?

   Membrane distillation shows the potential to create a gas that can be fed as fuel to an SOFC directly on the conditions of a preceding concentration step, operation in a low temperature range (25 to 35 °C) and under basic conditions ($pH > 10$). To conclude on whether it is a suitable technique within the *From pollutant to power* project, however, it must be considered in combination with the results of research on concentration technologies and SOFC performance.

   (a) What is the permeate quantity that can be obtained (at selected test conditions)?
   Obtained absolute total fluxes at the chosen test conditions of pH 10, Re 500 and partial vacuum pressure of 1500 Pa were about 7, 12, 20 and 27 kg/m^2/h for temperatures of 25, 35, 45 and 55 °C, respectively. Absolute fluxes do not show large variation for the different TAN concentrations within the applied range.

   (b) What is the permeate quality that can be obtained (at selected test conditions)?
   A permeate quality higher than 10 m% NH_3 (minimum proven SOFC fuel gas quality) were be obtained at low temperatures of 25 and 35 °C and for a high TAN concentration of 20 g TAN/L. Permeate quality between 5 m% NH_3 and 10 m% NH_3 (which might also suffice as SOFC fuel gas) were obtained at temperatures of 25, 35 and 45 °C for TAN concentrations of 12 and 20 g/L.

   (c) What are considerations regarding energy?
   An overall mass and energy balance in the *From pollutant to power* project could show

whether the SOFC electrical and thermal energy suffice to perform concentration and gas extraction steps with the produced gas, that is, whether an overall energy neutral or producing system could be created. Thus, an overall mass and energy balance for the *From pollutant to power* project would be needed to decide on whether MD is a suitable technology for gas production within the project. It could be beneficial to perform VMD at the lower temperatures that were found to be required to obtain an SOFC fuel with sufficient fuel quality in this study, as this would decrease the energy demand for heating of the feed solution.

Chapter 7

Recommendations for further research

Further optimization of the MD set-up is recommended, for example on the reduction of mass transfer resistance induced by temperature and concentration polarization effects. Also, an SGMD configuration could be considered. Literature shows lower fluxes but higher NH_3 selectivity for SGMD compared to VMD [25]. Usually, air is used as sweeping gas in SGMD configurations. However, as oxygen in air is an oxidator, air is not allowed in SOFCs. Possibly, SOFC off-gases could be used as sweeping gas. Moreover, partial vacuum pressures induced on the permeate side of MD membranes closer to the vapor pressure of water might result in higher selectivity and thus in higher permeate quality [12,17].

When a selective pervaporation membrane with preference for ammonia transport can be used instead of a non-selective, hydrophobic MD membrane, higher selectivities could be obtained [13]. So far, pervaporation research in relation to ammonia removal has not shown stable membrane performance on longer term and for temperatures higher than room temperature. [13] Further research on pervaporation for the production of ammonia gas and comparison with MD performance is recommended.

Thus far, the H_2O flux that comes with NH_3 flux has been considered as unfavorable. However, advantages may be discovered during SOFC research, for example, it could possibly function as a cooling mechanism for the heat produced in the SOFC. Otherwise, it is recommended to research an extra treatment step after MD to increase permeate quality. Condensation of permeate H_2O or multiple MD stages after each other might be options for this.

MD should be tested for real reject water or urine compositions, or at least for matrices that can be expected after a concentration step. Possible fouling mechanisms should be investigated, although not much (irreversible) fouling is expected due to the hydrophobic character of the membrane and the fact that MD is operated at atmospheric pressure.

Bibiliography

[1] Project Proposal STW-IWT Bilateral Projects 2014-2015, N2kWh – from Pollutant to Power.

[2] Van Linden, N. (2016. October). *N2kWh: From pollutant to power.* Scientific poster.

[3] Environmental Dynamics International (2011). *Aeration Efficiency Guide*

[4] European Parliament and the council (2008, November). Directive 2008/98/EC.

[5] EU Legislation in Progress (2017, February). *Circular economy package: Four legislative proposals on waste.*

[6] Zwart, M. M. (2014). From Pollutant to Fuel. A proof of principle for electricity production using nitrogen from sewage as a fuel.

[7] Takaya, N., Catalan-Sakairi, M. A. B., Sakaguchi, Y., Kato, I., Zhou, Z., & Shoun, H. (2003). Aerobic denitrifying bacteria that produce low levels of nitrous oxide. *Applied and environmental microbiology*, *69*(6), 3152-3157.

[8] [Niels van Linden (2017, March). Internal project results SOFC Tests Lausanne]

[9] STOWA (2012) Handboek slibgisting, rapport 2011-16, ISBN 978.90.5773.522.6

[10] Burton, F. L., Stensel, H. D., & Tchobanoglous, G. (Eds.). (2014). *Wastewater engineering: treatment and recovery*. McGraw-Hill.

[11] El-Bourawi, M. S., Khayet, M., Ma, R., Ding, Z., Li, Z., & Zhang, X. (2007). Application of vacuum membrane distillation for ammonia removal. *Journal of Membrane Science*, *301*(1), 200-209.

[12] El-Bourawi, M. S., Ding, Z., Ma, R., & Khayet, M. (2006). A framework for better understanding membrane distillation separation process. *Journal of membrane science*, *285*(1), 4-29.

[13] Yang, X., Fraser, T., Myat, D., Smart, S., Zhang, J., Diniz da Costa, J. C., ... & Duke, M. (2014). A pervaporation study of ammonia solutions using molecular sieve silica membranes. *Membranes*, *4*(1), 40-54.

[14] Lawson, K. W., & Lloyd, D. R. (1997). Membrane distillation. *Journal of membrane Science*, *124*(1), 1-25.

[15] Xie, Z., Duong, T., Hoang, M., Nguyen, C., & Bolto, B. (2009). Ammonia removal by sweep gas membrane distillation. *Water research*, *43*(6), 1693-1699.

[16] Hirabayashi, Y. (2002). Pervaporation membrane system for the removal of ammonia from water. *Materials Transactions*, *43*(5), 1074-1077.

[17] Chiam, C. K., & Sarbatly, R. (2013). Vacuum membrane distillation processes for aqueous solution treatment—A review. *Chemical Engineering and Processing: Process Intensification*, *74*, 27-54.

[18] Pangarkar, B. L., Thorat, P. V., Parjane, S. B., & Abhang, R. M. (2010). Performance evaluation of vacuum membrane distillation for desalination by using a flat sheet membrane. *Desalination and Water Treatment*, *21*(1-3), 328-334.

[19] Souhaimi, M. K., & Matsuura, T. (2011). *Membrane distillation: principles and applications*. Elsevier.

[20] Zarebska, A., Romero Nieto, D., Christensen, K. V., Fjerbæk Søtoft, L., & Norddahl, B. (2015). Ammonium fertilizers production from manure: a critical review. *Critical Reviews in Environmental Science and Technology*, *45*(14), 1469-1521.

[21] Xie, Z., Duong, T., Hoang, M., Nguyen, C., & Bolto, B. (2009). Ammonia removal by sweep gas membrane distillation. *Water research*, *43*(6), 1693-1699.

[22] Lu, J., Li, B., Wang, L., Wang, Y., & Wang, S. (2014). Utilization of ammonia-containing wastewater by combining membrane absorption and vacuum membrane distillation. *Journal of Chemical Technology and Biotechnology*, *89*(2), 312-321.

[23] Shim, S. M., Lee, S. J., & Kim, W. S. (2013). Experimental study on the performance evaluation of vacuum distillation process for NH4HCO3 removal. *Journal of Mechanical Science and Technology*, *27*(4), 1171-1178.

[24] Yang, X., Pang, H., Zhang, J., Liubinas, A., & Duke, M. (2017). Sustainable waste water deammonification by vacuum membrane distillation without pH adjustment: Role of water chemistry. *Chemical Engineering Journal*, *328*, 884-893.

[25] Ding, Z., Liu, L., Li, Z., Ma, R., & Yang, Z. (2006). Experimental study of ammonia removal from water by membrane distillation (MD): the comparison of three configurations. *Journal of membrane Science*, *286*(1), 93-103.

[26] Wu, C., Yan, H., Li, Z., & Lu, X. (2016). Ammonia recovery from high concentration wastewater of soda ash industry with membrane distillation process. *Desalination and Water Treatment*, *57*(15), 6792-6800.

[27] Duong, T., Xie, Z., Ng, D., & Hoang, M. (2013). Ammonia removal from aqueous solution by membrane distillation. *Water and Environment Journal*, *27*(3), 425-434.

[28] He, Q., Yu, G., Tu, T., Yan, S., Zhang, Y., & Zhao, S. (2017). Closing CO2 loop in biogas production: recycling ammonia as fertilizer. *Environmental Science & Technology*, *51*(15), 8841-8850.

[29] Zhao, Z. P., Xu, L., Shang, X., & Chen, K. (2013). Water regeneration from human urine by vacuum membrane distillation and analysis of membrane fouling characteristics. *Separation and Purification Technology*, *118*, 369-376.

[30] Fang, M., Ma, Q., Wang, Z., Xiang, Q., Jiang, W., & Xia, Z. (2015). A novel method to recover ammonia loss in ammonia-based CO2 capture system: ammonia regeneration by vacuum membrane distillation. *Greenhouse Gases: Science and Technology*, *5*(4), 487-498.

[31] Udert, K. M., Larsen, T. A., Biebow, M., & Gujer, W. (2003). Urea hydrolysis and precipitation dynamics in a urine-collecting system. *Water Research*, *37*(11), 2571-2582.

[32] Lind, B. B., Ban, Z., & Bydén, S. (2001). Volume reduction and concentration of nutrients in human urine. *Ecological Engineering*, *16*(4), 561-566.

[33] Tian, X., Wang, G., Guan, D., Li, J., Wang, A., Li, J., ... & Zhang, Z. (2016). Reverse osmosis brine for phosphorus recovery from source separated urine. *Chemosphere*, *165*, 202-210.

[34] Jenicek, P., Svehla, P., Zabranska, J., LeBlanc, R. J., Laughton, P. J., & Tyagi, R. (2007). Reject water treatment by nitritation/denitritation process–influence of ammonia concentration and loading rate. *Query GMSC*, 683-690.

[35] Release on the Ionization Constant of H_2O (The International Association for the Properties of Water and Steam, 2007)

[37] Sawyer, C. N., & McCarty, P. L. (1967). Chemistry for sanitary engineers. In *Chemistry for sanitary engineers*. McGraw-Hill.

[38] Tan, Z. (2014). *Air pollution and greenhouse gases: from basic concepts to engineering applications for air emission control*. Springer.

[39] Parkhurst, D. L., & Appelo, C. A. J. (2013). *Description of input and examples for PHREEQC version 3: a computer program for speciation, batch-reaction, one-dimensional transport, and inverse geochemical calculations* (No. 6-A43). US Geological Survey.

[40] You, W. T., Xu, Z. L., Dong, Z. Q., & Zhao, Y. J. (2014). Separated performances of ammonium sulphate and ammonium chloride solutions treated by vacuum membrane distillation. *The Canadian Journal of Chemical Engineering*, *92*(7), 1306-1313.

[41] Chemical Thermodynamics (Rock, 1969)

[42] Introduction to Chemical Engineering Thermodynamics (Smith et al., 2005)

[43] Mojab, S. M., Pollard, A., Pharoah, J. G., Beale, S. B., & Hanff, E. S. (2014). Unsteady laminar to turbulent flow in a spacer-filled channel. *Flow, turbulence and combustion*, *92*(1-2), 563-577.

[44] Da Costa, A. R., Fane, A. G., & Wiley, D. E. (1994). Spacer characterization and pressure drop modelling in spacer-filled channels for ultrafiltration. *Journal of membrane science*, *87*(1-2), 79-98.

[45] Schock, G., & Miquel, A. (1987). Mass transfer and pressure loss in spiral wound modules. *Desalination*, *64*, 339-352.

[46] Hendricks, D. W. (2006). *Water treatment unit processes: physical and chemical*. CRC press.

[47] Zhani, K., Zarzoum, K., Ben Bacha, H., Koschikowski, J., & Pfeifle, D. (2016). Autonomous solar powered membrane distillation systems: state of the art. *Desalination and Water Treatment*, *57*(48-49), 23038-23051.
[48] Onsekizoglu, P. (2012). Membrane distillation: principle, advances, limitations and future prospects in food industry. In *Distillation-Advances from Modeling to Applications*. InTech.
[49] Khayet, M., & Matsuura, T. (2004). Pervaporation and vacuum membrane distillation processes: modeling and experiments. *AIChE journal*, *50*(8), 1697-1712.
[50] Hickey, P. J., & Gooding, C. H. (1994). Mass transfer in spiral wound pervaporation modules. *Journal of Membrane science*, *92*(1), 59-74.)
[52] Pronk, W., Biebow, M., & Boller, M. (2006). Electrodialysis for recovering salts from a urine solution containing micropollutants. *Environmental science & technology*, *40*(7), 2414-2420.
[53] [Internal results of the N2kWh project by Rob Deckers and Christiaan Hordijk]
[54] De Moel, P. J., Van Dijk, J. C., & Van der Meer, W. (2012). Waterchemie voor drinkwater modeleren met PHREEQc. *H2O, 45 (3), 2012*.
[55] https://www.sterlitech.com/cf042-crossflow-cell-cf042ac.html
[56] Pangarkar, B. L., Thorat, P. V., Parjane, S. B., & Abhang, R. M. (2010). Performance evaluation of vacuum membrane distillation for desalination by using a flat sheet membrane. *Desalination and Water Treatment*, *21*(1-3), 328-334.
[57] Miyawaki, O., Saito, A., Matsuo, T., & Nakamura, K. (1997). Activity and activity coefficient of water in aqueous solutions and their relationships with solution structure parameters. *Bioscience, biotechnology, and biochemistry*, *61*(3), 466-469.
[58] Casagrande, C. G., Kunz, A., De Prá, M. C., Bressan, C. R., & Soares, H. M. (2013). High nitrogen removal rate using ANAMMOX process at short hydraulic retention time. *Water Science and Technology*, *67*(5), 968-975.
[59] Wilsenach, J. A. (2006). Treatment of source separated urine and its effects on wastewater systems.
[60] Reig, M., Casas, S., Aladjem, C., Valderrama, C., Gibert, O., Valero, F., ... & Cortina, J. L. (2014). Concentration of NaCl from seawater reverse osmosis brines for the chlor-alkali industry by electrodialysis. *Desalination*, *342*, 107-117.
[61] Smil, V. (2004). *Enriching the earth: Fritz Haber, Carl Bosch, and the transformation of world food production*. MIT press.
[62] IWA Resource Recovery Cluster. *State of the Art Compendium Report on Resource Recovery from Water.*
[63] Strous, M., Van Gerven, E., Zheng, P., Kuenen, J. G., & Jetten, M. S. (1997). Ammonium removal from concentrated waste streams with the anaerobic ammonium oxidation (anammox) process in different reactor configurations. *Water Research*, *31*(8), 1955-1962.
[64] Szatkowska, A. B., & Paulsrud, B. The anammox process for nitrogen removal from wastewater–achievements and future challenges.
[65] Magrí, A., Béline, F., & Dabert, P. (2013). Feasibility and interest of the anammox process as treatment alternative for anaerobic digester supernatants in manure processing–An overview. *Journal of environmental management*, *131*, 170-184.
[66] Elvers, B. (1989). *Ullmann's encyclopedia of industrial chemistry* (pp. 173-174). S. Hawkins, & W. Russey (Eds.). Verlag Chemie.
[67] STOWA (2012). Explorative research on innovative nitrogen recovery, rapport 51, ISBN 978.90.5773.585.1
[68] Ni, M., Leung, M. K., & Leung, D. Y. (2009). Ammonia-fed solid oxide fuel cells for power generation—A review. *International Journal of Energy Research*, *33*(11), 943-959.
[69] Kendall, K., & Kendall, M. (2015). *High-temperature Solid Oxide Fuel Cells for the 21st Century: Fundamentals, Design and Applications*. Elsevier.

[70] Fuerte, A., Valenzuela, R. X., Escudero, M. J., & Daza, L. (2009). Ammonia as efficient fuel for SOFC. *Journal of Power Sources*, *192*(1), 170-174.
[71] Wilsenach, J. A., & Van Loosdrecht, M. C. (2004). Effects of separate urine collection on advanced nutrient removal processes. *Environmental science & technology*, *38*(4), 1208-1215.
[72] Ma, S., Wang, J., Yan, Z., Dai, Y., & Lu, B. (2011). Thermodynamic analysis of a new combined cooling, heat and power system driven by solid oxide fuel cell based on ammonia–water mixture. *Journal of Power Sources*, *196*(20), 8463-8471.
[73] Wojcik, A., Middleton, H., & Damopoulos, I. (2003). Ammonia as a fuel in solid oxide fuel cells. *Journal of Power Sources*, *118*(1), 342-348.
[75] Appelo, C. A. J., & Postma, D. (2004). *Geochemistry, groundwater and pollution*. CRC press.
[76] Cohen, P. (1989). *The ASME handbook on water technology for thermal power systems* (No. DOE/NE/34076-T4; EPRI-GS--6303). American Society of Mechanical Engineers, New York, NY (USA).
[77] Garrels and Christ (1965) Activity of H2O in saline water.
[78] Mook W (2000) Chemistry of carbonic acid in water. In 'Environmental Isotopes in the Hydrological Cycle: Principles and Applications' pp. 143-165. (INEA / UNESCO: Paris). [1] Retrieved 30NOV2013.
[79] Peng, J., & Wan, A. (1998). Effect of ionic strength on Henry's constants of volatile organic compound. *Chemosphere*, *36*(13), 2731-2740.
[80] Yurteri, C., Ryan, D. F., Callow, J. J., & Gurol, M. D. (1987). The effect of chemical composition of water on Henry's law constant. *Journal (Water Pollution Control Federation)*, 950-956.
[81] Zhang, J., Duke, M., Xie, Z., & Gray, S. (2010). Performance of asymmetric hollow fibre membranes in membrane distillation under various configurations and vacuum enhancement. *Journal of Membrane Science*, *362*(1), 517-528.
[82] Mengual, J. I., Khayet, M., & Godino, M. P. (2004). Heat and mass transfer in vacuum membrane distillation. *International Journal of Heat and Mass Transfer*, *47*(4), 865-875.
[83] Pitzer, K.S., 1981. Characteristics of very concentrated aqueous solutions. In F.E. Wickman and D.T. Rickard (eds), *Chemistry and geochemistry of solutions at high temperatures and pressures*. *Phys. Chem. Earth* 3 and 4, 249–272.
[84] Mani, K. N. (1991). Electrodialysis water splitting technology. *Journal of membrane science*, *58*(2), 117-138.
[85] Speight, J. G. (2005). *Lange's handbook of chemistry* (Vol. 1). New York: McGraw-Hill.

Appendices

A Solid oxide fuel cells

A1 Cell and reactions

Solid oxide fuel cells consist of an anode, a cathode and an electrolyte that separates them. Solid oxide fuel cells are operated at high temperatures of about 700 °C, at which NH_3 is cracked into N_2 and H_2 at the anode in the presence of a nickel catalyst. At the cathode, O_2 is reduced. O^{2-} migrates from the cathode to the anode through the electrolyte. At the anode, it reacts with the H_2 that resulted from cracking to form H_2O and electrons.

Anode, cathode and overall reactions are:

Cathode reaction

O_2 reduction: $\frac{1}{2}\,O_2 + 2\,e^- \rightarrow O^{2-}$

Anode reactions

NH_3 cracking: $NH_3 \rightarrow \frac{1}{2}\,N_2 + \frac{3}{2}\,H_2$

H_2 oxidation: $H_2 + O^{2-} \rightarrow H_2O + 2\,e^-$

Overall reaction

NH_3 oxidation: $NH_3 + \frac{3}{4}\,O_2 \rightarrow \frac{3}{2}\,H_2O + \frac{1}{2}\,N_2$

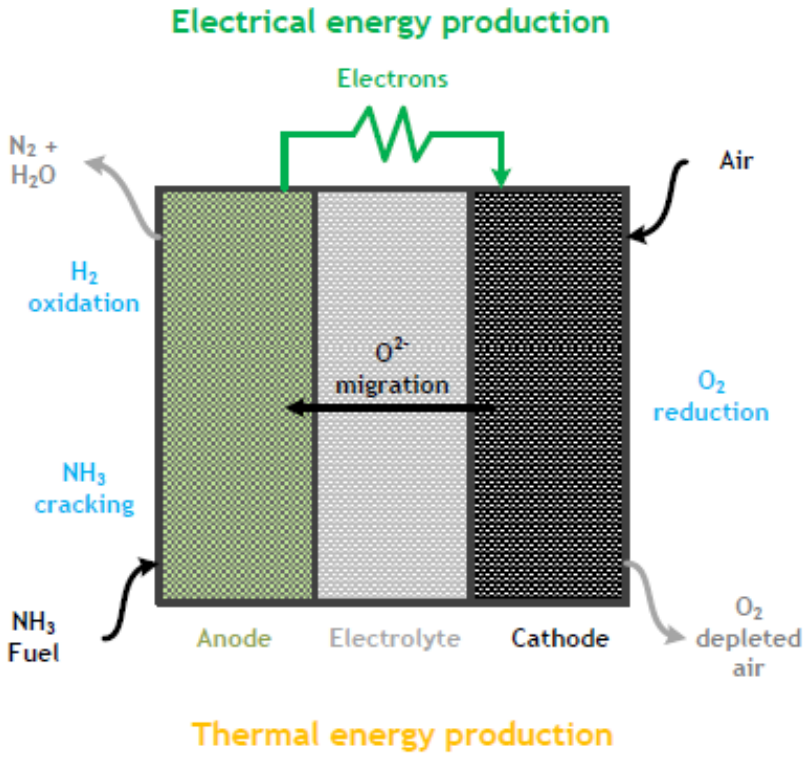

Solid oxide fuel cell [2]

A2 Initial SOFC test results

Initial tests feeding fuel gas containing NH_3 to an SOFC have been carried out within the *From pollutant to power* project. Gaseous fuels containing NH_3 and H_2O with NH_3 mass percentages (defined as $mass_{NH3}/mass_{total}$) of 5, 10 and 25% have been introduced to an SOFC. Performances in terms of power and electrical potential are shown in the figure below, as well as the performance of a 100% H_2 gas. The results show that SOFCs work well on the gases with 10 and 25 NH_3 mass percentages, but not on the 5% gas.

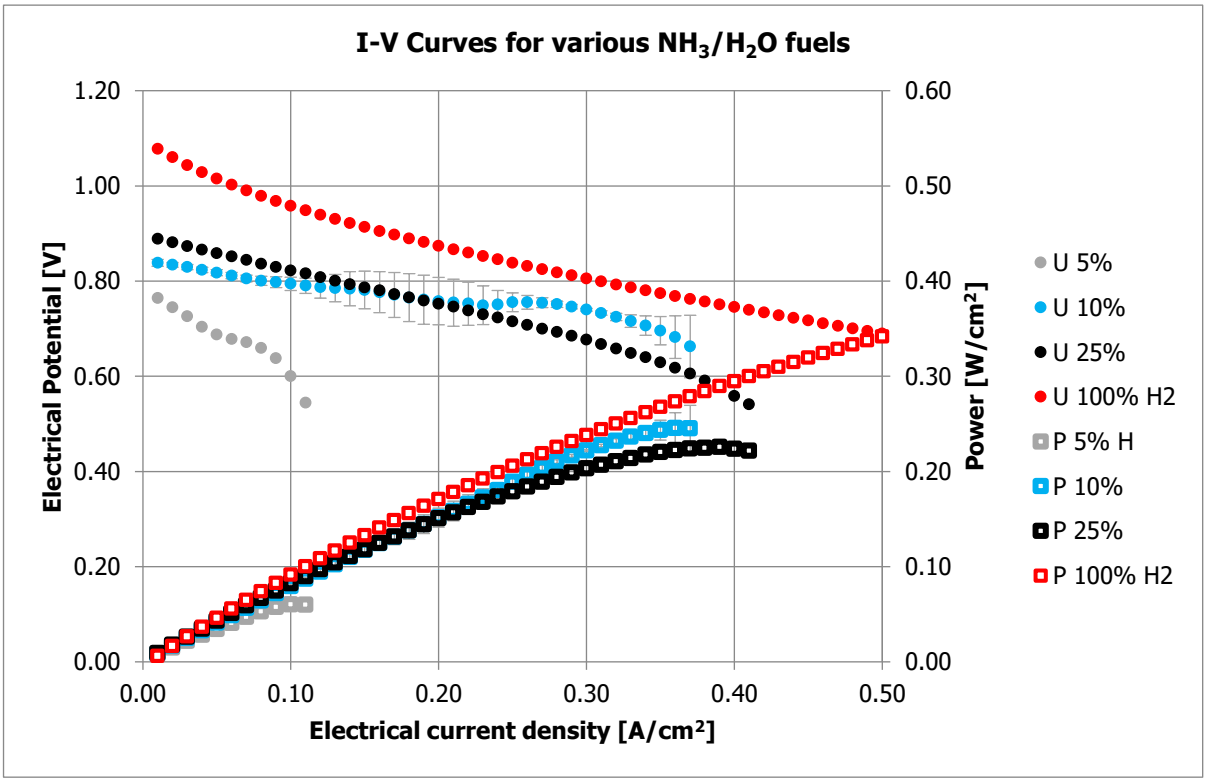

Initial SOFC test results [8]

B Derivations and calculations related to hydrodynamic conditions

B1 Hydraulic diameter for spacer-filled channels formula derivation

The derivation of the formula for hydraulic diameter calculation for spacer-filled channels is based on information obtained from [43-45].

For flow channels with periodically variable cross sections, such as spacer-filled flow channels, the following definition for the hydraulic diameter (d_H) is generally applied:

$$d_h = \frac{4 \cdot \text{volume of flow channel}}{\text{wetted surface}}$$

When the volume of the flow channel is defined as the volume of the flow channel without the spacer (V_{tot}) minus the volume occupied by the spacer (V_{sp}), and the wetted surface is defined as the sum of the surfaces of the flow channel (S_{FC}) and the spacer material (S_{sp}), the definition can be written as:

$$d_h = \frac{4(V_{tot} - V_{sp})}{S_{FC} + S_{sp}} = \frac{4(V_{tot} - V_{sp})}{S_{FC} + S_{sp}} \cdot \frac{\frac{1}{V_{tot}}}{\frac{1}{V_{tot}}} = \frac{4\frac{(V_{tot} - V_{sp})}{V_{tot}}}{\frac{S_{FC}}{V_{tot}} + \frac{S_{sp}}{V_{tot}}}$$

Definitions of voidage (ε) and spacer specific surface (S_{vsp}) and rewritings and combination of these definitions allow further elaboration of d_H:

$$\varepsilon = \frac{\text{void volume}}{\text{total volume}} = \frac{V_{tot} - V_{sp}}{V_{tot}} = 1 - \frac{V_{sp}}{V_{tot}} \qquad \rightarrow \qquad \frac{V_{sp}}{V_{tot}} = 1 - \varepsilon$$

$$S_{vsp} = \frac{S_{sp}}{V_{sp}}$$

$$(1 - \varepsilon) \cdot S_{vsp} = \frac{V_{sp}}{V_{tot}} \cdot \frac{S_{sp}}{V_{sp}} = \frac{S_{sp}}{V_{tot}} \qquad \rightarrow \qquad \frac{S_{sp}}{V_{tot}} = (1 - \varepsilon) \cdot S_{vsp}$$

The height, width and length of the flow channel are defined as h, b and l, respectively. With this information, d_H can be written as:

$$d_h = \frac{4\varepsilon}{\frac{2l(h+b)}{hbl} + (1 - \varepsilon) \cdot S_{vsp}} = d_h = \frac{4\varepsilon}{\frac{2(h+b)}{hb} + (1 - \varepsilon) \cdot S_{vsp}}$$

For a flat channel, b>>h. This allows the following reduction:

$$d_h = \frac{2(h+b)}{hb} \approx \frac{2b}{hb} = \frac{2}{h}$$

Thus, d_H can be written as:

$$d_h = \frac{4\varepsilon}{\frac{2}{h} + (1 - \varepsilon) \cdot S_{vsp}}$$

In order to calculate d_H, ε and S_{vsp} have to be determined first. ε is the most important geometric characteristic of spacers, mathematically incorporating the mesh size, filament diameter and angle between filaments. From the definition given above, it can be concluded that ε can be calculated after determination of V_{sp} and V_{tot}.

In the general case, a spacer with a parallelogram type mesh and filaments of different sizes is considered (figure below). The volume of the spacer is calculated for a mesh by:

$$V_{sp} = \frac{1}{2}\left\{\frac{2\pi d_{f1}^2 l_{m2}}{4} + \frac{2\pi d_{f2}^2 l_{m1}}{4}\right\} = \frac{\pi}{4}\left(d_{f1}^2 l_{m2} + d_{f2}^2 l_{m1}\right)$$

The first term in the brackets represents the volume of the thin filament and the second the volume of the thick filament. The cross-sections of the filaments are assumed to be circular, with a surface of $¼\pi d^2$. The length of the filaments in a mesh are As two of each type of filaments contributes to the volume in a mesh, both terms are multiplied by 2. Moreover, the terms are multiplied by the filament lengths in a mesh (l_m). The factor ½ corrects for the fact that each filament is part of two adjacent meshes.

V_{tot} is the product of the mesh area (S_{mesh}) and the spacer thickness(h_{sp}):

$$V_{tot} = S_{mesh} h_{sp}$$

S_{mesh} can be calculated as:

$$S_{mesh} = l_{m2} l_{m1} \sin\theta$$

In this formula, Θ is the angle between the filaments (figure below). Both ε and d_H are functions of Θ. Since a mesh is characterized by two supplementary angles with the same sine it is irrelevant which angle is used. h_{sp} is the spacer thickness and is equal to the height of the spacer-filled channel, but usually less than the sum of df_1 and df_2 because filaments can be slightly embedded in each other.

Combining the formulas gives us:

$$V_{tot} = l_{m2} * l_{m1} * h * \sin\theta$$

and:

$$\varepsilon = 1 - \frac{\pi(d_{f1}^2 l_{m2} + d_{f2}^2 l_{m1})}{4 * l_{m2} * l_{m1} * h * \sin\theta}$$

For the simplest case of a rhombic mesh ($lm_1 = lm_2 = lm$) and the filaments have equal diameters ($df_1 = df_2 = df$), the equation can be reduced to:

$$\varepsilon = 1 - \frac{\pi d_f^2}{2 * l_m * h * \sin\theta}$$

With the definition of S_{vsp} as given previously, only S_{sp} is left to be defined for calculation of d_H. For the general case, S_{sp} can be calculated by:

$$S_{sp} = \frac{1}{2}\{2\pi d_{f1} l_{m2} + 2\pi d_{f2} l_{m1}\}$$

Also in this formula, the factor ½ corrects for the fact that each filament is part of two adjacent meshes.

For a rhombic type mesh with single size filaments, this reduces to:

$$S_{sp} = 2\pi d_f l_m$$

and

$$V_{sp} = \frac{\pi}{2} d_f^2 l_m$$

Together, these are used for calculation of S_{vsp}:

$$S_{vsp} = \frac{2\pi d_f l_m}{\frac{\pi}{2} d_f^2 l_m} = \frac{4}{d_f}$$

Thus, for a rhombic type mesh, d_H can be calculated as:

$$d_h = \frac{4\varepsilon}{\frac{2}{h} + \frac{4(1-\varepsilon)}{d_f}}$$

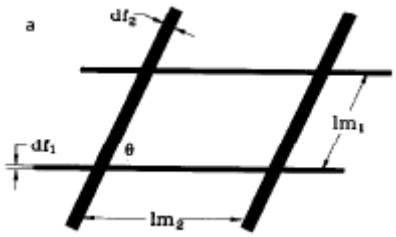

Definitions of df_1, df_2, lm_1, lm_2 and Θ

B2 Required cross flow velocity in experimental set-up

The dimensions and characteristics of the used spacer and channel are given in the table below.

Channel width (b)	[m]	0.0392
Channel height (hcavity)	[m]	0.0023
Number of spacers	[-]	1
Spacer thickness (hsp)	[m]	0.0016 m
Spacer filament thickness (df)	[m]	0.00063
Distance between filaments on a layer (lm)	[m]	0.003
Θ	[rad]	1.57
Spacer volume (Vsp)	[m3]	6.99E-07
Total volume (Vtot)	[m3]	7.74E-06
Void volume fraction (ε)	[-]	9.10E-01
Spacer surface (Ssp)	[m2]	4.44E-03
Spacer specific surface (Svsp)	[1/m]	6.35E03
Hydraulic diameter (dH)	[m]	0.0025

The required cross flow velocity can be recalculated from the Reynolds number, kinematic viscosity and hydraulic diameter:

$$u_{required} = \frac{Re \cdot \nu}{D} = \frac{Re \cdot \nu}{d_h}$$

With the selected Reynolds number of Re = 500, the following mean interstitial velocities were calculated for temperatures of 20 to 70 °C in steps of 10 °C:

T [°C]	μ [kg/m/s]	ρ [kg/m^3]	Mean interstitial velocity (u) [m/s]
20	0.001002	998.2	0.199
30	0.000798	995.7	0.159
40	0.000653	992.2	0.131
50	0.000547	988.1	0.110
60	0.000467	983.2	0.094
70	0.000404	977.8	0.082

As the real densities and viscosities were not known, density and viscosity of water were used. Pump speeds for temperatures of 25, 35, 45 and 55 degrees were derived from the relation between pump speed and mean interstitial velocities for the temperatures of 20, 30, 40, 50, 60 and 70 °C. The relation between mean interstitial velocity and pump speed was derived from pump calibration.

C PHREEQC

C1 TAN equilibrium 12 and 20 g TAN/L

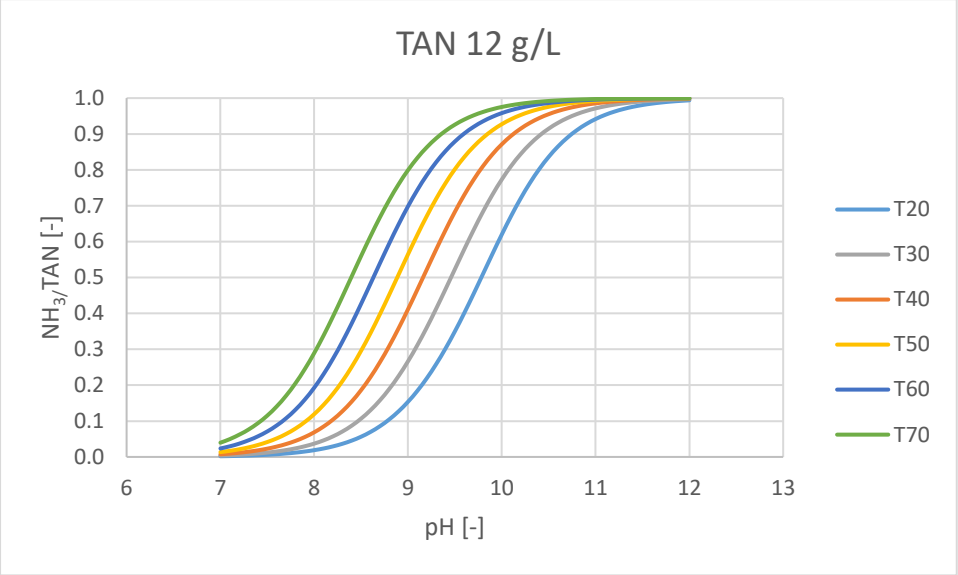

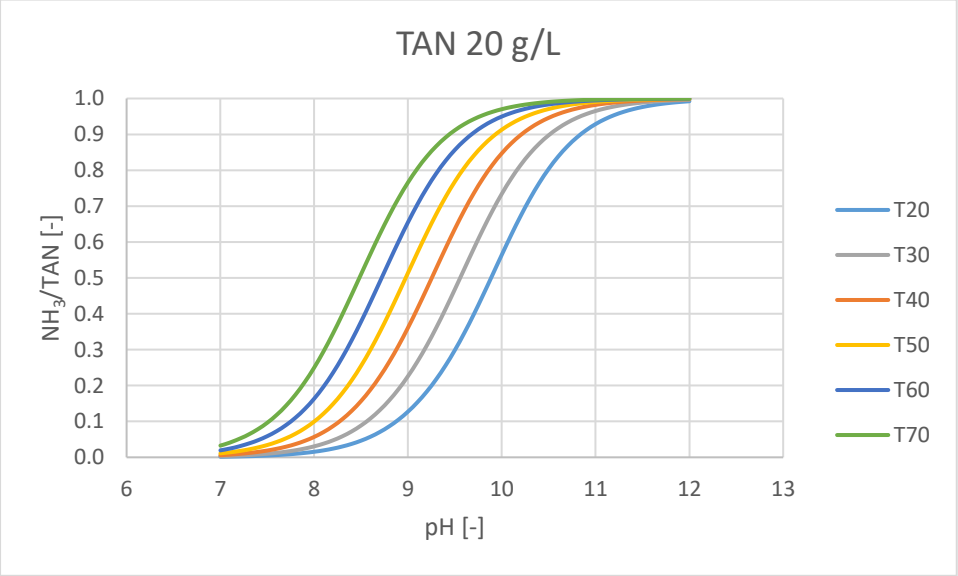

C2 PHREEQC validation by manual calculations for the TAN equilibrium

The Gibbs free energy *change* (ΔG) is the driving force that causes a system to pass from an initial state to a final state. ΔG is the difference between the G of the final state and the G of the initial state:

$\Delta G = \Delta G_{final} - \Delta G_{initial}$

$\Delta G = 0$ equilibrium
$\Delta G < 0$ spontaneous process from initial to final (that is; spontaneous if $\Delta G_{final} < \Delta G_{initial}$)

The sign of ΔG depends on the enthalpy change ΔH (heat released or absorbed during process), the entropy change ΔS (disorder of a system) and the temperature of the system via the Gibbs-Helmholtz equation:

$\Delta G = \Delta H - \Delta S \cdot T$

For a specific compound, we use the ΔG for the reaction by which that compound is formed, under standard conditions (i.e. T = 298 K and p = 1.0 atm). We call this the standard free energy of formation (ΔG^0_f)

For a chemical reaction involving reactants and products, the ΔG for the reaction can be derived. For a reaction:

$aA + bB \leftrightarrow cC + dD,$

$\Delta G = \Delta G^0 + RT \cdot LN(([C]^c \cdot [D]^d / ([A]^a \cdot [B]^b)) = \Delta G^0 + RT \cdot LN(K)$

where K is the equilibrium constant. Strictly, activities should be used instead of concentrations. However, in aqueous solutions with low ionic strength concentrations may be used.

In this equation, ΔG^0 is the energy that is released from or needs to be put into a chemical reaction. It is the difference between the standard free energies of formation of the initial and the final state of the reaction:

$\Delta G^0 = \Sigma \Delta G^0_f$(formed components) - $\Sigma \Delta G^0_f$(removed components). Logically, the amounts of formed and removed components should be taken into account.

In equilibrium, there is no driving force anymore as the system has reached its final state. This means that ΔG = 0 and therefore that $\Delta G^0 = -RT \cdot LN(K)$.

ΔG^0_R(reaction) = ΣG^0_f(products) - ΣG^0_f(reactants)
ΔH^0_R(reaction) = ΣH^0_f(products) - ΣH^0_f(reactants)
ΔS^0_R(reaction) = ΣS^0_f(products) - ΣS^0_f(reactants)

The subscript *f* refers to the formation values (standard free energy of formation), that may be obtained from handbooks for most elements and compounds (e.g. *Lide's Handbook of Chemistry and Physics* and *Lange's Handbook of Chemistry*). For compounds of interest to water treatment, textbooks (e.g. Grady et al. 1999 and Rittman and McCarty 2001) or papers (McCarty 1975) provide such data with examples on how to calculate ΔG^0_R(reaction). The designation, "standard" values mean that the values were obtained under "standard" conditions, meaning T = 298 K and p = 1.0 atm. *Molar concentrations A, B, C and D are 1.*

The values for ΔG, ΔH and ΔS without the ^{0} superscript mean that they pertain to "physiological" conditions, i.e., whatever conditions occur in the cell or externally as may be the case,

ΔG_R(reaction) = ΣG_f(products) - ΣG_f(reactants)
ΔH_R(reaction) = ΣH_f(products) - ΣH^0_f(reactants)
ΔS^0_R(reaction) = ΣS^0_f(products) - ΣS^0_f(reactants)

For a given reaction,

aA + bB ←→ cC + dD,

ΔG_R(reaction) = [c·G_f(C) + d·G_f(D)] – [a·G_f(A) + b·G_f(B)]

where G_f(A) is the Gibbs free energy of formation of component A (kJ/mol A) etc.

For the TAN equilibrium, this means:

NH4+ ← → NH3 + H+

$\Delta G^0_{reaction}$ is calculated at standard state or reference case (T = 298.15, p = 1 atm), and from this K = EXP(-$\Delta G^0_{reaction}$/(RT))

Assuming that enthalpy change is constant over the small temperature range we look at, values for K at different temperatures can be calculated as:

LN(K2/Kref) = -ΔH^0/R*(1/T2-1-Tref) → K2 = Kref * EXP(-ΔH^0/R*(1/T2-1-Tref))

When we know K, the ratio NH3/TAN can be calculated for any pH:

K = [NH3]*[H+]/[NH4+] and [TAN} = [NH4+] + [NH3]

[NH4] = [TAN] – [NH3]

K = [NH3]*[H+]/([TAN] – [NH3])

K*([TAN] – [NH3]) = [NH3]*[H+]

K*[TAN] – K*[NH3] = [H+]*[NH3]

K*[TAN] = [H+]*[NH3]+K*[NH3]

K*[TAN] = ([H+] + K)*[NH3]

K/([H+] + K) = [NH3]/[TAN]

And:

pH = -log([H+])

-pH = log([H+])

[H+] = 10^(-pH)

Therefore:

[NH3]/[TAN] = K/(10^(-pH)+K)

Manual calculations and PHREEQC calculations have been carried out for an ammonia solution of 1 g NH_3/L over pH for temperatures 10 to 70 °C. Thermodynamic data used from [85].

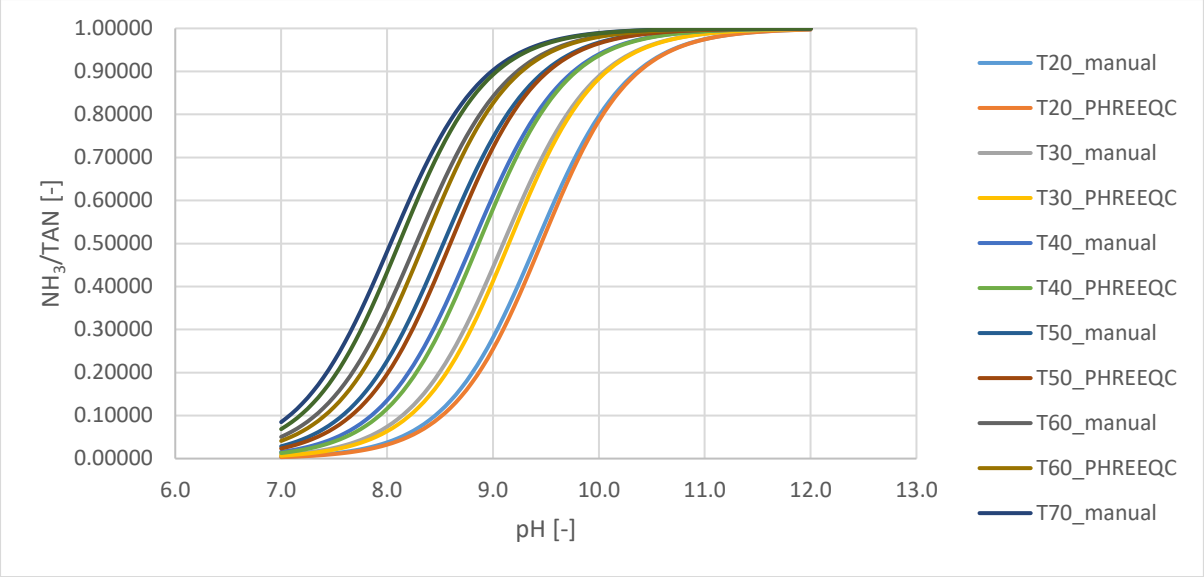
1.00000
0.90000
0.80000
0.70000
0.60000
0.50000
0.40000
0.30000
0.20000
0.10000
0.00000
NH3/TAN [-]
6.0
7.0
8.0
9.0
10.0
11.0
12.0
13.0
pH [-]
T20_manual
T20_PHREEQC
T30_manual
T30_PHREEQC
T40_manual
T40_PHREEQC
T50_manual
T50_PHREEQC
T60_manual
T60_PHREEQC
T70_manual

C3 PHREEQC validation by literature data and manual calculations for vapor pressures

Vapor pressure calculations based on the SI resulted from PHREEQC simulations is validated with literature data for water and with manual calculations for an ammonia (NH_4OH) solution.

Water:

For H2O, simulations for the vapor pressure of water only have been taken from *CRC Handbook of Chemistry and Physics* (David R. Lide, ed. (2005)). The H2O vapor pressure as determined from PHREEQC and as determined from literature differ less than 1% in the considered temperature range from 20 to 70 °C.

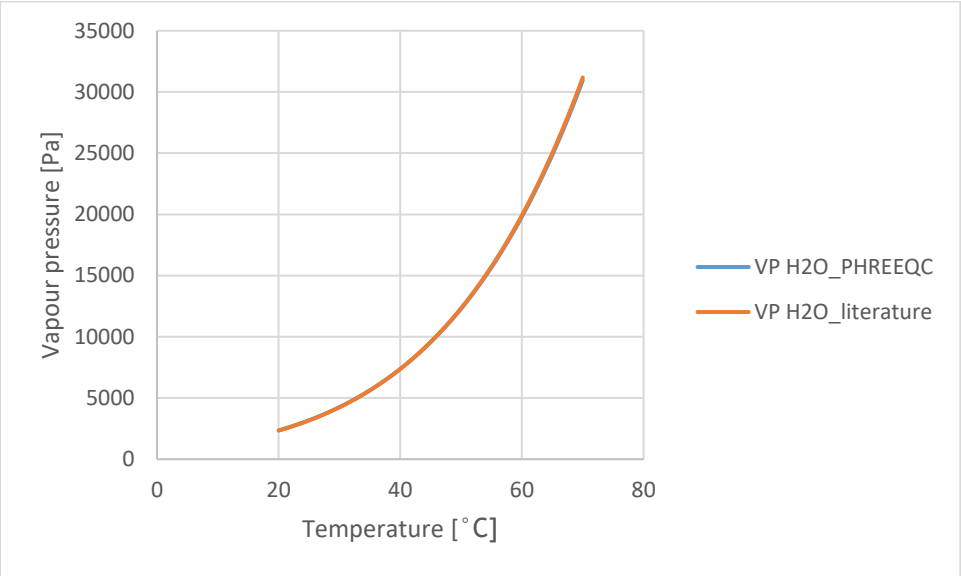

Ammonia solution:

Equilibrium vapor pressures have been calculated for a NH_4OH solution applying Henry's Law in solubility form for TAN concentrations of 1, 6, 12 and 20 g/L. As the natural pH of NH_4OH is high, it is assumed that all TAN is present in the form of NH_3.

A reference Henry's Law constant at a reference temperature (T_{ref}) and an exponential relationship of K_H = EXP(-8.09694+3917.507/T-0.00314*T) are used, which is a form derived from the Van 't Hoff equation valid over a temperature range from 0 to 40 °C (obtained from http://pubs.acs.org/doi/abs/10.1021/j100357a041?journalCode=jpchax).

T_{ref} is 298.15 K and KH at T_{ref} is 61 M/atm.

Differences between results from PHREEQC simulations and manual calculations differ less than 10% within the temperature range of 20 to 40 °C. For higher temperatures the differences become larger, which is explained by the fact that the used relationship between Henry's Law constant and temperature is not valid anymore.

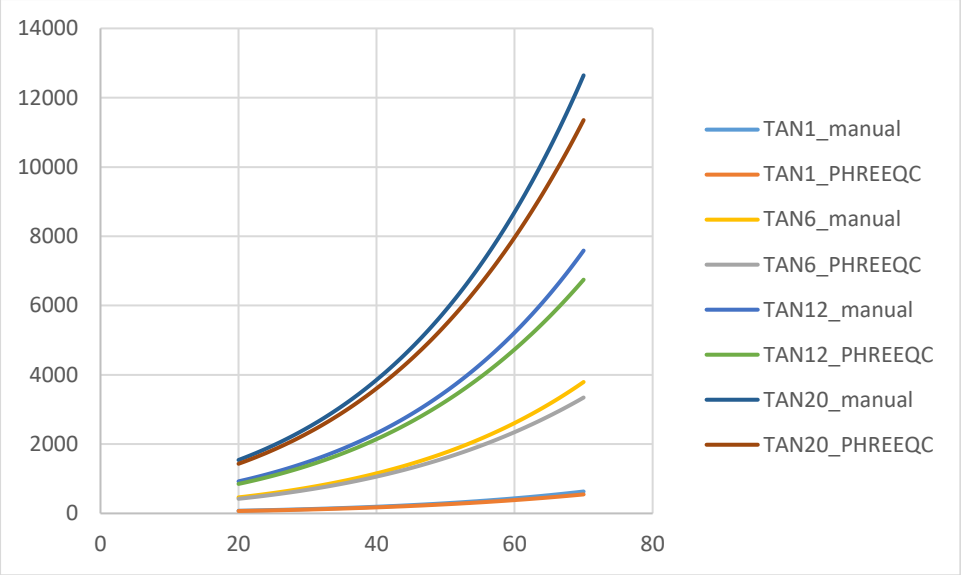
14000
12000
10000
8000
6000
4000
2000
0
0
20
40
60
80
TAN1_manual
TAN1_PHREEQC
TAN6_manual
TAN6_PHREEQC
TAN12_manual
TAN12_PHREEQC
TAN20_manual
TAN20_PHREEQC

D Vapor pressure simulation results

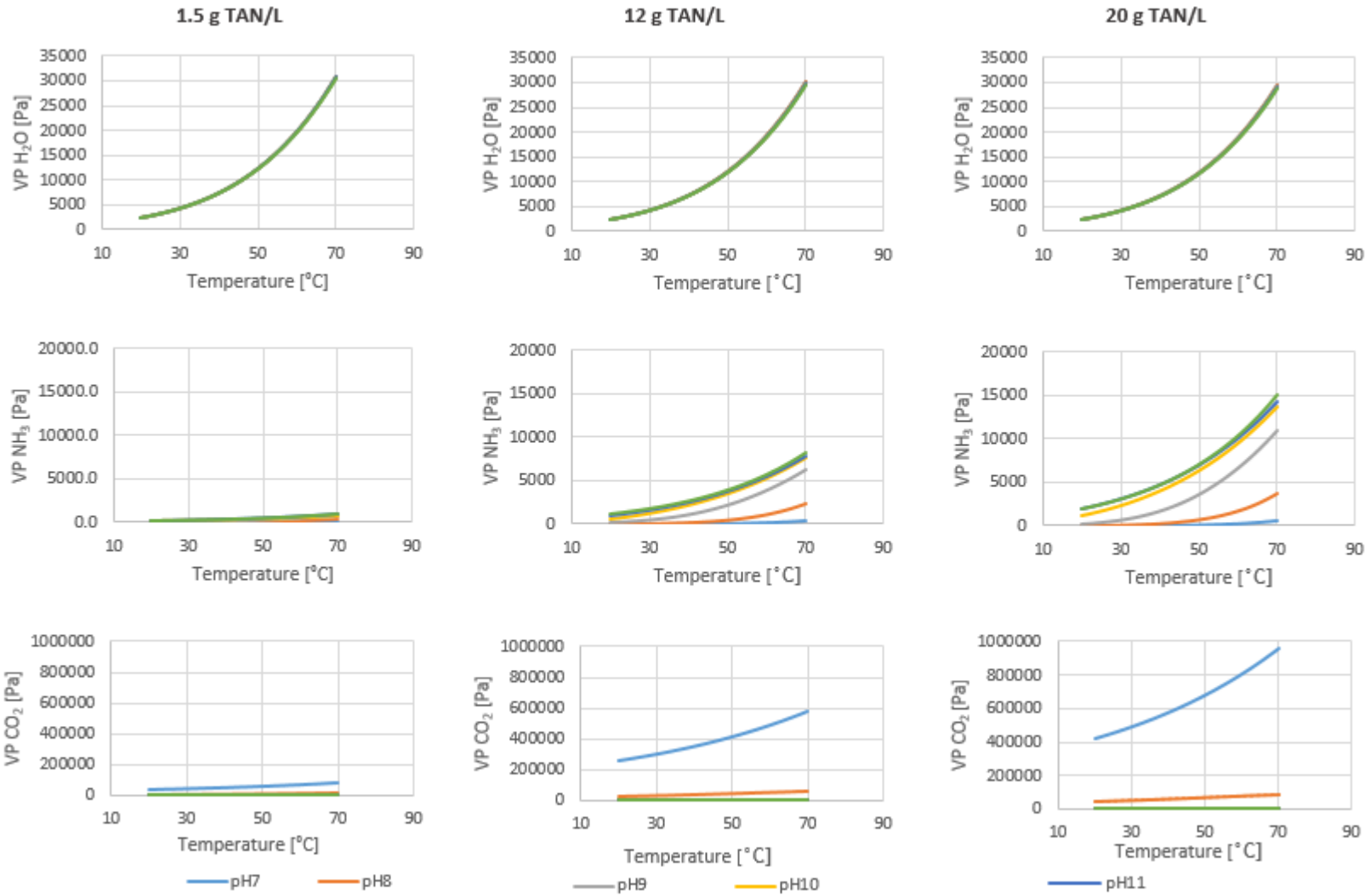

E Electrodialysis with bipolar membranes

Internal results from the *From pollutant to power* project show that it is possible to obtain a pH of 10 with the use of bipolar membranes in electrodialysis. The NH_4HCO_3 concentrations in the legend next to the graph refer to concentrations in the initial base stream. pH 10 has been obtained for a NH_4HCO_3 concentration of 0 g/L, which was a NaCl solution. pH increase in this solution is stronger than in NH_4HCO_3 initial base streams due to the absence of buffer capacity.

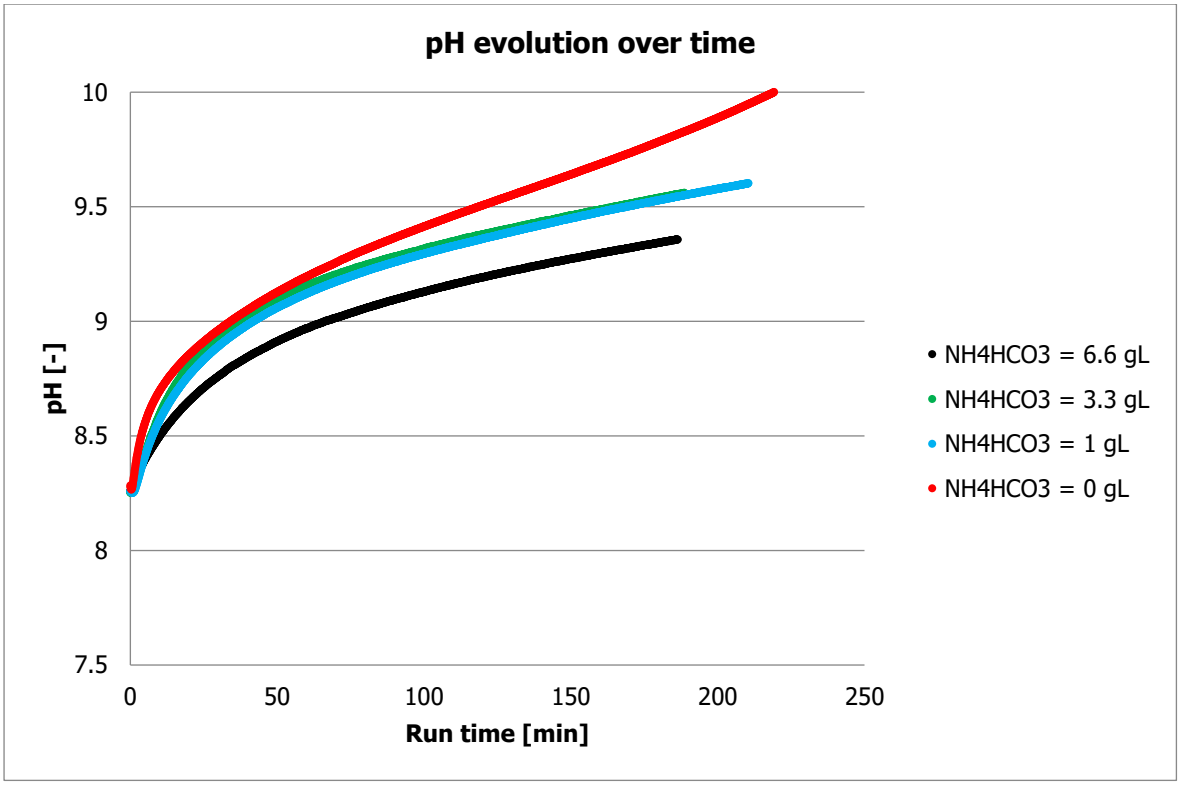

F Initial and final parameter values

	Run time [h]	Initial demiwater volume [g]	Initial pH [-]	Initial EC [µS/cm]	Initial C_{TAN} [g/L]	Final pH [-]	Final EC [µS/cm]	Final C_{TAN} [g/L]
TAN1.5 _T25 _1	1.23	650.9	10.07	13940	1.49	9.90	14360	0.95
_2	1.50	650.5	10.04	13760	1.67	9.84	14260	0.92
_T35 _1	1.50	650.5	10.09	15340	1.52	10.03	17100	0.62
_2	1.50	650.6	10.16	15680	1.45	10.10	17390	0.58
_T45 _1	1.83	1034.8	10.03	15210	1.71	9.93	17660	0.84
_2	1.83	1034.9	9.99	15510	1.61	9.98	17850	0.81
_T55 _1	1.50	645.1	10.03	45600	6.85	9.90	57900	2.49
_2	1.98	644.7	10.01	54500	4.11	9.86	64100	0.75
TAN12 _T25 _1	1.50	560.0	10.04	60000	11.44	9.74	61500	7.35
_2	1.50	560.2	10.01	60500	10.94	9.76	62000	7.32
_T35 _1	1.50	1001.6	10.03	70000	14.61	9.77	74100	11.12
_2	1.25	930.6	9.99	65100	11.99	9.88	67600	8.82
_T45 _1	1.65	562.5	9.95	72900	15.09	9.69	85000	6.95
_2	1.50	563.0	10.08	72700	14.79	9.857	83100	7.72
_T55 _1	2.00	584.2	9.86	74000	15.07	9.47	95900	7.11
_2	2.00	564.7	10.22	76000	16.32	10.06	96300	6.36
TAN20 _T25 _1	1.50	520.1	10.12	84800	20.11	9.86	86800	14.53
_2	1.50	520.0	9.99	85100	20.12	9.73	86600	14.73
_T35 _1	1.50	520.1	10.11	87500	24.64	9.92	93700	14.93
_2	1.50	520.0	10.04	88700	23.40	9.89	95600	14.04
_T45 _1	1.50	519.8	10.03	88800	24.45	9.79	99500	15.28
_2	1.50	520.0	10.06	89700	23.28	9.92	99800	16.23
_T55 _1	1.50	510.8	9.97	84900	24.67	9.66	100600	16.60
_2	1.53	517.4	9.94	86300	24.52	9.69	101400	15.49